

1 **Adakites without a slab: Remelting of hydrous basalt in the crust and shallow mantle of**  
2 **Borneo to produce the Miocene Sintang Suite and Bau Suite magmatism of West Sarawak**

3 H. Tim Breitfeld<sup>1</sup>, Colin Macpherson<sup>2</sup>, Robert Hall<sup>1</sup>, Matthew Thirlwall<sup>3</sup>, Chris J. Ottley<sup>2</sup>, Juliane  
4 Hennig-Breitfeld<sup>1</sup>

5 <sup>1</sup> *SE Asia Research Group, Department of Earth Sciences, Royal Holloway University of London,*  
6 *Egham, Surrey, TW20 0EX, United Kingdom*

7 <sup>2</sup> *Department of Earth Sciences, University of Durham, Durham, DH1 3LE, United Kingdom*

8 <sup>3</sup> *Department of Earth Sciences, Royal Holloway University of London, Egham, Surrey, TW20 0EX,*  
9 *United Kingdom*

10

11 Key words: adakites; Sintang Suite; Bau Suite; intraplate magmatism; zircon U-Pb geochronology;  
12 Sarawak; Borneo

13

14 **Abstract**

15 We present new geochronological and geochemical data for Neogene magmatism from West  
16 Sarawak. Zircon U-Pb geochronology divides Neogene magmatic rocks of West Sarawak into a Lower  
17 Miocene West Sarawak Sintang Suite with ages of c. 19 to 21 Ma, and a Middle Miocene Bau Suite  
18 with ages of c. 12 to 14 Ma. Magmatism occurred in multiple short-lived pulses from approximately  
19 24 Ma and was coeval with magmatic activity in NW Kalimantan and East Kalimantan. The majority  
20 of, but not all, Bau Suite samples display adakitic chemistry, while the West Sarawak Sintang Suite is  
21 predominantly non-adakitic. There was no active subduction zone or subducted slab associated with  
22 this adakitic magmatism. Instead, the geochemical diversity is consistent with the Bau and West  
23 Sarawak Sintang suites representing mixtures of mafic, mantle-derived magma with felsic magma  
24 derived from remelting of hydrous, mafic rock that had been emplaced into the lithosphere of  
25 Borneo as arc basalt tens or hundreds of millions of years previously. This origin is most evident in  
26 the main Sintang Suite of central Borneo (Kalimantan) which has preserved less contaminated

27 examples of the mafic endmember. This endmember resembles basaltic rocks from several locations  
28 across Borneo suggesting that intraplate, mantle-derived magmatism was responsible for remelting  
29 older, hydrated basaltic rocks in the crust.

## 30 **1. Introduction**

31 Subduction zones have been major sites of crustal processing since at least the Neoproterozoic.  
32 While there is debate about early Precambrian geodynamics, including the role and importance of  
33 subduction (Stern, 2005; van Hunen and Moyen, 2012), modern subduction zones have produced, so  
34 called, adakitic magmatic rocks that resemble the tonalite – trondhjemite – granodiorite (TTG) suites  
35 which are common constituents of felsic Archean terranes (Campbell and Taylor, 1983; Kelemen,  
36 1995; Drummond et al., 1996). Therefore, understanding the genesis of adakitic rocks is an  
37 important step in understanding the development of the Earth’s continental crust.

38 Adakites were initially interpreted as melts derived from young subducted oceanic crust (Defant and  
39 Drummond et al., 1990), but there have since been many studies that have found adakitic rocks  
40 either in subduction zones lacking subducted young oceanic lithosphere (e.g. Sajona et al., 1993;  
41 Castillo et al., 1999; Macpherson et al., 2006), or formed by melting of basaltic rock in the highly  
42 thickened crust of collision zones (Chung et al., 2003; Hou et al., 2004; Guo et al., 2007). Thus,  
43 several different processes – some involving slab melting, some not – have been proposed to explain  
44 the generation of the adakitic chemical signature. Each of these has implications for the geodynamic  
45 settings in which adakites are found and potentially for processes that might have been common  
46 during the Archean.

47 In this paper, we explore the temporal, petrological, and geochemical development of a suite of  
48 Neogene magmatic rocks from Borneo that includes adakitic rocks. These were generated in a  
49 setting that had lacked subduction during, at least, the preceding 50 million years, and where there  
50 is no evidence of substantial crustal thickening. We show that these adakites were  
51 contemporaneous with (i) non-adakitic granodiorites which were derived from similar sources to the  
52 adakites, and (ii) mantle-derived magmas resembling ocean island basalts. This indicates that the  
53 hydrated basaltic source of the adakites was present in the Borneo lithosphere, and implies  
54 subduction before the Oligo-Miocene, but there was no active subduction zone or subducted slab  
55 associated with the adakitic melts, which probably resulted from intraplate processes.

## 56 **2. Regional background**

57 The Kuching Zone in Borneo of Haile (1974), extending from the Lupar Line in the north to the  
58 Schwaner Mountains in the south (Fig. 1 and 2), includes Palaeozoic to Cenozoic metamorphic,  
59 sedimentary and igneous rocks (e.g. Liechti et al., 1960; Hutchison, 2005; Breifeld et al., 2017,  
60 2018). The upper Cenozoic in the Kuching Zone is characterised by widespread, small igneous  
61 intrusions which form the focus of this study (Fig. 2). Geochemically similar rocks from Kalimantan  
62 and West Sarawak (Kirk, 1968; Williams and Harahap, 1987) are predominantly of Late Oligocene to  
63 Early Miocene age, and have been referred to as the Sintang Intrusives, the Sintang Intrusive Suite or  
64 the Sintang Suite (e.g. Dutch, 1992; Moss et al., 1998; Hutchison, 2005, 2010). We follow Hutchison  
65 in preferring the term Sintang Suite because not all of the igneous rocks are intrusive.

### 66 *2.1. Pre-Oligocene magmatism in Borneo*

67 The extensive Schwaner Mountains granitic batholith, which lies immediately south of the area of  
68 Sintang Suite magmatism (Fig. 2) formed during Cretaceous subduction that ceased at around 90 to  
69 80 Ma (Pieters and Sanyoto, 1993; Hutchison, 1996; Moss, 1998; Hall, 2012; Davies et al., 2014;  
70 Breifeld et al., 2017; Hennig et al., 2017). Subsequent minor magmatic episodes produced the upper  
71 Cretaceous Pueh and Gading batholiths of West Sarawak (Kirk, 1968; Hennig et al., 2017; Fig. 3), the  
72 Eocene Muller Volcanics, Nyaan Volcanics, Piyabung Volcanics and Serantak Volcanics in NW and  
73 central Kalimantan (Pieters et al., 1987; Bladon et al., 1989; Fig. 2), and the Eocene Piring stock in  
74 North Sarawak (Hennig-Breifeld et al., 2019; Fig. 3) .

### 75 *2.2. Sintang Suite: Upper Oligocene to Lower Miocene magmatism in Borneo*

76 The Upper Oligocene to Lower Miocene Sintang Suite consists of small sills, stocks and dykes, which  
77 form distinctive topographic features across a broad swathe of western Borneo (Williams and  
78 Harahap, 1987 and references therein) between the Schwaner Mountains and the Lupar Line (Fig. 2).  
79 Compositions are predominantly dacitic, granodioritic, or subordinately dioritic to granitic, with I-  
80 type character (Williams and Harahap, 1987). Whole-rock, biotite, and hornblende K-Ar dating of 12

81 samples collected near Sintang in NW Kalimantan (Williams and Harahap, 1987) yielded two distinct  
82 age groups: an older group of 30.4 to 23 Ma in the Melawi Basin near Sintang (type locality), and a  
83 younger group of 17.9 to 16.4 Ma in the Ketungau Basin. One biotite age of c. 42 Ma was excluded  
84 as it came from a rock which intruded probable Oligocene sediments. The NW Kalimantan Sintang  
85 Suite includes geochemically distinctive Northern, Central and Southern groups (Harahap, 1993;  
86 Heryanto et al., 1993), which are retained in this study (Fig. 2).

87 In West Sarawak the Sintang Suite comprises sills (Fig. 4a), lava flows (Fig. 4b and d), dykes (Fig. 4c)  
88 and stocks which intrude the Kayan Sandstone and sediments of the northern Ketungau Basin. Kirk  
89 (1968) reported K-Ar biotite ages of  $16 \pm 4$  Ma at Gunung Rawan and  $19 \pm 3$  Ma at Pulau Satang (Fig.  
90 3), while Schmidtke et al. (1990) reported K-Ar hornblende ages of  $17.2 \pm 1.9$  for an intrusion south  
91 of Kuching and  $25.8 \pm 1.9$  Ma for the Serapi dyke (Fig. 3). Prouteau et al. (1996, 2001) reported  
92 whole-rock K-Ar ages in West Sarawak of 22.3 to 23.7 Ma for calc-alkaline diorites and microdiorites  
93 in northern West Sarawak. These display similar geochemical diversity to the NW Kalimantan Sintang  
94 Suite, which they identified as having partly adakitic chemistry.

### 95 *2.3. Northeast and East Kalimantan*

96 In East Kalimantan K-Ar mica ages of 17.5 to 19.4 Ma (Bladon et al., 1989), and 21 to 24 Ma  
97 (Setiawan and Le Bel, 1987), as well as a Rb-Sr age of 26 Ma (Hutchison, 2010) were reported for the  
98 Long Laai granite province (Fig. 2). Van de Weerd et al. (1987) and van Leeuwen et al. (1990)  
99 reported K-Ar ages of 14.4 to 24 Ma for basic igneous rocks associated with gold mineralisation in  
100 the Kelian area, which are part of the Kalimantan gold belt. Andesites in the Kelian area yielded U-Pb  
101 zircon ages of 19 to 20 Ma (Setiabudi et al., 2001, 2007) and are intruded by rhyolites with U-Pb  
102 zircon ages of 19.5 to 19.8 Ma (Davies, 2002; Davies et al., 2008). K-Ar ages of 18 to 23 Ma for  
103 magmatic rocks near the Telen and Malnyu Rivers (northern Kutai Basin) were included in the  
104 Sintang Suite by Moss et al. (1998), Soeria-Atmadja et al. (1999) and Cullen et al. (2013), but we

105 retain distinct location names (e.g. Kalimantan gold belt, Long Laai, Telen/Malnyu) in view of their  
106 significant spatial separation from our study area (Fig. 2).

#### 107 *2.4. Bau Suite: Middle to Upper Miocene magmatism*

108 Intrusions around the town of Bau (Figs. 2 and 3), West Sarawak, have been dated as Middle to Late  
109 Miocene age. Therefore, this Bau Suite is younger than the Sintang Suite and magmatism in East and  
110 North Kalimantan. JICA (1985) reported whole-rock K-Ar ages of 10 to 12 Ma for quartz porphyries  
111 while Prouteau et al. (2001) reported whole-rock K-Ar ages of 6.4 to 14.6 Ma for microtonalites and  
112 dacites near Kuching and Bau, which they also classified as adakites. The Bau Suite is associated with  
113 gold mineralisation of Carlin-type (Percival et al., 1990; Schuh and Guilbert, 1990), and includes  
114 disseminated sediment hosted gold deposits within the Bau Limestone and the adjacent Pedawan  
115 Formation (e.g. Jugan field) (Schuh, 1993; Kirwin and Royle, 2018).

#### 116 *2.5. Geodynamic Setting of the Sintang Suite*

117 A broad swathe of Borneo, including West Sarawak, experienced Sintang Suite magmatism from the  
118 Late Oligocene (Fig. 2) but the causes are not clear. Dating is limited, with most ages from K-Ar  
119 whole rock dating, and there has been limited geochemical study of this suite. A subduction-related  
120 origin was inferred by Hamilton (1979), Prouteau et al. (1996, 2001), Soeria-Atmadja (1999), and  
121 Hartono (2006) but, despite their widespread distribution, the Sintang rocks occur as small isolated  
122 bodies located far from any potential Oligo-Miocene subduction zone. Others have proposed post-  
123 collisional or post-subduction settings (Kirk, 1968; Williams and Harahap, 1987; Moss et al., 1998;  
124 Zaw et al., 2011).

125 Hutchison (1996) introduced the term Sarawak Orogeny to explain a major tectonic change in NW  
126 Borneo in the Late Eocene, to which Prouteau et al. (2001) attributed the Sintang Suite magmatism,  
127 but recent studies have questioned the implied collisional event (Hall, 2012; Hall and Sevastjanova,  
128 2012; Hall and Breitfeld, 2017; Hennig-Breitfeld et al., 2019). Early tectonic models (e.g. Taylor and  
129 Hayes, 1983) suggested an Early Miocene collision in northern Borneo, from Sarawak to Sabah, but

130 later work indicates that subduction beneath Sarawak west of the West Baram Line (Fig. 2) ceased in  
131 the Cretaceous at around 90 to 80 Ma (Williams et al., 1988; Moss, 1998; Hall & Spakman, 2015;  
132 Breitfeld et al., 2017; Hennig et al., 2017) although deep marine sedimentation continued until the  
133 Late Eocene (Galini et al., 2017; Breitfeld & Hall, 2018). Between the Late Eocene and Early Miocene,  
134 to the west of the West Baram Line, NW Borneo was an elevated region (Hall, 2013; Hennig-Breitfeld  
135 et al., 2019), and offshore and onshore Sarawak were extensive coastal and shelf areas (e.g.  
136 Hageman, 1987; Madon, 1999; Hassan et al., 2013). There is no evidence of a late Paleogene or  
137 Neogene subduction margin in Sarawak and subduction was restricted to Sabah, east of the West  
138 Baram Line, between the Late Eocene and Early Miocene (Hall, 2013; Hall and Spakman, 2015; Hall  
139 and Breitfeld 2017). Thus, there is no evidence for active subduction beneath west Borneo at the  
140 time of Sintang and Bau Suite magmatism.

141 We present below new geochemical data and U-Pb zircon ages from the Sintang and Bau suites of  
142 West Sarawak that show different pulses of magmatism. We integrate our new findings with  
143 published data to offer a new interpretation of their petrogenesis, and then discuss the origin of  
144 adakitic and non-adakitic geochemical characters in non-subduction environments.

145

### 146 **3. Methodology**

#### 147 *3.1. Sampling*

148 Fresh rocks or rocks with minimal alteration were sampled (TB samples) from outcrops or nearby  
149 float in West Sarawak (Fig. 3). Additional samples from Bau (BYG) were provided by Menzies Mining.  
150 Nine samples from the West Sarawak Sintang Suite and thirteen from the Bau Suite were analysed  
151 for geochemistry, and zircons from seven samples were separated for radiometric dating. All sample  
152 locations and type of analysis can be found in Supplementary Tab. 1.

153        *3.2. Geochemistry*

154 Whole rock geochemical analysis by X-ray fluorescence (XRF) was conducted at Royal Holloway  
155 University of London (RHUL; Tab. 1). Samples were processed with a jaw crusher and a tungsten-  
156 carbide mill to produce powders. XRF analyses were mostly performed using a PANalytical Axios  
157 sequential X-ray fluorescence spectrometer with 4kW Rh-anode X-ray tube, while Bau Suite BYG  
158 samples were analysed using the previous Philips PW1480 XRF. On this latter instrument, a W-anode  
159 X-ray tube was used to determine Ba, La, Ce, Nd, Ni, Cr, V, Sc, Cu and Zn whereas a Rh-anode tube  
160 was used for the major elements, Pb, Th, Rb, Sr, Y, Zr, Nb, Cl, and Ga. Major elements were  
161 measured on fusion discs using the La<sub>2</sub>O<sub>3</sub>-bearing Spectroflux 105, after ignition of both rock  
162 powders and flux at 1100°C. All concentrations are reported on a volatile-free basis. The heavy  
163 absorber La results in very small matrix corrections. SO<sub>3</sub> concentrations reported for samples  
164 analysed on the Axios reflect sulphur present as sulphate, as sulphide sulphur is largely volatilized  
165 during the fusion process. Trace elements were measured on pressed pellets, with matrix  
166 corrections calculated from the major elements. Ca and Ti were analysed on both pellets and discs  
167 to confirm that the same powder was used for both pellet and disc; the fusion disc data is of higher  
168 quality. An artificial glass bead was analysed every third sample to correct for instrumental drift,  
169 which was at the <1 % level on the Axios, and a few % on the PW1480, where the drift monitor was  
170 analysed for each element following the sample analyses for that element. 30 to 40 international  
171 rocks standards were used for calibration. Calibration graphs are publicly available at  
172 <https://www.royalholloway.ac.uk/research-and-teaching/departments-and-schools/earth->  
173 [sciences/research/research-laboratories/x-ray-fluorescence-laboratory/](https://www.royalholloway.ac.uk/research-and-teaching/departments-and-schools/earth-sciences/research/research-laboratories/x-ray-fluorescence-laboratory/). The quality of the straight  
174 line fit of these graphs is the best indicator of accuracy over a wide range of concentrations. Where  
175 there is more scatter, this can reflect poor precision of the XRF analyses relative to the calibrated  
176 concentration range (e.g. Sn, where precision is about ±2 ppm, and the calibrated range only 15  
177 ppm); inaccuracies in the published standard data (e.g. S, Cl), or inaccuracies in the XRF data (e.g. at  
178 <100 ppm F). Precision of the XRF data is a function of detection limit at low concentrations, and of

179 count rate at higher concentrations; this means that the concentration uncertainty is an absolute  
180 concentration at low levels, and a percentage concentration at higher levels. Estimates of these  
181 parameters are given in Tab. 1. An example of pellet reproducibility, and comparison between XRF  
182 and isotope dilution data, are given in the web link referred to above.

183 A wider range of trace elements were determined for BYG samples in the Department of Earth  
184 Sciences at Durham University using Inductively Coupled Plasma Mass Spectroscopy (ICP-MS) on a  
185 Perkin Elmer Elan 6000 following the procedure of Ottley et al. (2003). Briefly, 4 ml HF and 1 ml  
186 HNO<sub>3</sub> (SPA, ROMIL Cambridge) was added to 100 mg of powdered sample and sealed in a teflon vial  
187 on a hot plate at 150°C for 48 hours. The acid mixture was evaporated to near dryness followed by  
188 two cycles of adding a further 1 ml of HNO<sub>3</sub> and evaporation to near dryness. Finally, 2.5 ml HNO<sub>3</sub>  
189 was added and diluted to 50 ml after the addition of an internal Re and Rh standard to final  
190 concentrations of 20 ppb each. The internal standard allows compensation for analytical drift and  
191 matrix suppression effects. ICP-MS analyses were calibrated using international rock standards  
192 (BHVO1, AGV1, W2) which, along with analytical blanks, were prepared using the same procedure as  
193 samples. Reproducibility was monitored via replicate analysis of reference standards throughout the  
194 analysis sequence with % RSD always <3 % RSD, and typically <2 % RSD and by comparison of trace  
195 element analyses of ICP-MS with XRF (Supplementary Tabs. 2.1 and 2.2).

### 196 *3.3. Zircon separation*

197 A 63-250 µm fraction of zircon was separated at RHUL. This was purified using heavy liquids sodium  
198 polytungstate (SPT) and lithium heteropolytungstate (LST) at a density of 2.89 g/cm<sup>3</sup> and a FRANTZ  
199 magnetic barrier separator, followed by additional heavy liquid separation with di-iodomethane  
200 (DIM) at 3.3 g/cm<sup>3</sup> and hand picking of zircons. Grains were mounted in epoxy resin blocks and  
201 polished to expose mid-grain sections. Analysis spots for each grain were selected using transmitted  
202 light and cathodoluminescence scanning electron microscope (SEM-CL) images to avoid cracks and  
203 inclusions.

#### 204 3.4. LA-ICP-MS U-(Th)-Pb dating

205 Zircon U-Pb geochronology was performed at the Birkbeck College, University of London (UCL), using  
206 New Wave NWR 193 (25  $\mu\text{m}$  spot size) and New Wave NWR 213 nm (30  $\mu\text{m}$  spot size) laser ablation  
207 (LA) systems coupled to an Agilent 7700 quadrupole-based plasma ICP-MS with a two-cell sample  
208 chamber. The Plešovice zircon standard ( $337.13 \pm 0.37$  Ma; Sláma et al., 2008) and a NIST 612 silicate  
209 glass bead (Pearce et al., 1997) were used to correct for instrumental mass bias and depth-  
210 dependent inter-element fractionation of Pb, Th and U. GLITTER (Griffin et al., 2008) data reduction  
211 software was used. The data were corrected using the common lead correction method by Andersen  
212 (2002), which is used as a  $^{204}\text{Pb}$  common lead-independent procedure.

213 For grains older than 1000 Ma, the  $^{207}\text{Pb}/^{206}\text{Pb}$  ratio is given and for grains younger than 1000 Ma,  
214 the  $^{238}\text{U}/^{206}\text{Pb}$  ratio is given, because  $^{207}\text{Pb}$  cannot be measured with sufficient precision in these  
215 samples resulting in large uncertainties on the age (Nemchin and Cawood, 2005). Ages greater than  
216 1000 Ma are considered to be concordant if the difference between the  $^{207}\text{Pb}/^{206}\text{Pb}$  and  $^{206}\text{Pb}/^{238}\text{U}$   
217 ages is <10%, and ages less than 1000 Ma were considered to be concordant if the  $^{207}\text{Pb}/^{235}\text{U}$  and  
218  $^{206}\text{Pb}/^{238}\text{U}$  age difference is <10%. For young ages a simple concordance test is insufficient (Nemchin  
219 and Cawood, 2005) as the concordance range is too small to test reliably. Instead all analyses <25  
220 Ma were considered for the age calculation, except analyses which were interpreted to be affected  
221 by lead loss, inheritance or common Pb.

222 Isoplot 4.11 (Ludwig, 2003) was used for graphical illustration of Tera-Wasserburg concordia  
223 diagrams (Tera and Wasserburg, 1972). Tera-Wasserburg plots were used to identify individual  
224 peaks or visually assess outliers (e.g. lead loss, inheritance and common lead) within the population  
225 which were then excluded from the weighted mean age calculation. The reject function of Isoplot  
226 was used to further exclude statistical outliers (Ludwig, 2003). The youngest significant population  
227 were interpreted as crystallisation ages and used to calculate the weighted mean age. U-Pb zircon  
228 data for each sample are presented in the Supplementary Tabs. 3.1 to 3.7 and a summary of

229 weighted mean ages is displayed in Tab. 2. Conventional concordia plots are given in Supplementary  
230 Fig. 2.

231

## 232 **4. Petrography**

### 233 *4.1. West Sarawak Sintang Suite*

#### 234 *4.1.1. Intrusive rocks*

235 Micro-tonalites/granodiorites (TB33, TB148a, STB36c, and STB61b) dominate the intrusive West  
236 Sarawak Sintang Suite. They are composed mainly of quartz, plagioclase, an opaque phase and alkali  
237 feldspar. Plagioclase is more abundant than alkali feldspar and both form large, zoned phenocrysts,  
238 commonly idiomorphic to hypidiomorphic. Larger plagioclase phenocrysts may be altered to  
239 epidote. The matrix consists of fine grained quartz, plagioclase and sericite. The composition of  
240 granodiorite TB58 closely resembles the micro-granodiorites/tonalites, but has a coarser grained  
241 phaneritic texture (Fig. 4e). Plagioclase occurs as abundant prismatic crystals (Fig. 4e). Scarce  
242 amphibole occurs as subhedral grains which show advanced epidote group mineral alteration (Fig.  
243 4f). Biotite occurs as brown and green varieties with only minor chlorite alteration (Fig. 4e). There is  
244 some sericite alteration of feldspar and biotite. More mafic monzodiorites and (gabbro-) diorites  
245 (TB23, TB231) contain plagioclase, alkali feldspar, biotite, epidote, amphibole, quartz and an opaque  
246 phase. Plagioclase and alkali feldspar form large idiomorphic to hypidiomorphic phenocrysts. Biotite  
247 is often replaced by sericite, chlorite and titanite. Amphiboles are subhedral and replaced by epidote  
248 group minerals and calcite.

#### 249 *4.1.2. Volcanic rocks*

250 Volcanic rocks of the West Sarawak Sintang Suite comprise felsic rhyolites to rhyodacites (TB18,  
251 TB141, TB176b, TB209a) and a mafic trachydacite (TB161). The felsic samples are porphyritic,  
252 containing idiomorphic to hypidiomorphic phenocrysts of quartz (Fig. 4g), alkali feldspar (Fig. 4h),  
253 and plagioclase (Fig. 4i), often zoned, in a very fine grained groundmass. Idiomorphic volcanic quartz

254 commonly has a bipyramidal shape, embayments and inclusions of sericite, biotite and plagioclase.  
255 Sericite alteration of the matrix is common. TB161 is a more mafic trachydacite with phenocrysts of  
256 biotite, plagioclase, epidote, pyroxene and quartz. Quartz is monocrystalline and unstrained with  
257 bipyramidal idiomorphic or hypidiomorphic shapes. Plagioclase and clinopyroxene form  
258 hypidiomorphic phenocrysts in a very fine grained altered matrix of sericite, plagioclase and epidote  
259 group minerals (Fig. 4j). Biotite is commonly chloritised.

#### 260 *4.2. Bau Suite*

261 Bau Suite samples are predominantly micro-granodiorites and micro-tonalites. Plagioclase, alkali  
262 feldspar and biotite form phenocrysts in a fine grained quartz and feldspar matrix. Plagioclase is  
263 zoned and forms idiomorphic to subidiomorphic crystals (Fig. 4k). Alkali feldspar is very rare, forming  
264 subidiomorphic crystals. Sericite alteration is common within feldspars, more so in alkali feldspar  
265 than plagioclase. Biotite commonly forms idiomorphic to subidiomorphic crystals (Fig. 4l), which may  
266 be heavily altered to sericite, epidote and titanite with chlorite rims. Hornblende forms idiomorphic  
267 to subidiomorphic crystals (Fig. 4m), but is uncommon.

268 A conspicuous feature of many Bau samples are large, resorbed quartz crystals. Up to 2 mm across,  
269 these display a variety of textures from slightly sub-angular to a majority which are highly rounded  
270 (Fig. 4m) or have scalloped margins. Some crystals also show evidence of newly-grown rims of  
271 microscopic quartz. Internal textures also vary from unstrained to significantly strained. In rare cases  
272 a number of quartz crystals, usually no more than 3 or 4, can be found together with contacts which  
273 suggest that they were part of a pre-existing quartz-rich mass. Together, these observations suggest  
274 that the Bau magma assimilated grains of a very quartz-rich lithology that has experienced various  
275 amounts of deformation and disaggregation.

276

277 **5. Geochemistry**

278 *5.1. West Sarawak Sintang Suite*

279 *5.1.1. Intrusive rocks*

280 Intrusive rocks of the West Sarawak Sintang Suite are predominantly felsic with a range of SiO<sub>2</sub>  
281 contents from 56 to 70 wt. %, classified as granodiorite, monzodiorite and gabbro-diorite  
282 (Supplementary Fig. 1). On the basis of their K<sub>2</sub>O contents of 1.28 to 2.65 wt. % (Tab. 1) they are calc-  
283 alkaline (Supplementary Fig. 1). According to the granite classification of Frost et al. (2001) they are  
284 magnesian calcic or magnesian calc-alkaline, peraluminous or metaluminous granitoids  
285 (Supplementary Fig. 1).

286 The new analyses show major element variations that are coherent with those previously recorded  
287 for Sintang Suite diorites from the Kuching area (Prouteau et al., 2001), but over a slightly wider SiO<sub>2</sub>  
288 range (Fig. 6). Al<sub>2</sub>O<sub>3</sub>, Fe<sub>2</sub>O<sub>3</sub>, MgO, CaO and TiO<sub>2</sub> decrease with increasing silica contents while K<sub>2</sub>O  
289 increases slightly and Na<sub>2</sub>O shows no systematic variation. Major element variations in the West  
290 Sarawak Sintang intrusive rocks are also coherent with those of Sintang intrusive rocks from  
291 Kalimantan (Fig. 5a). Like the Northern and Southern Kalimantan Sintang groups, West Sarawak  
292 Sintang intrusive rocks have a wider range of silica and slightly lower Al<sub>2</sub>O<sub>3</sub> and higher K<sub>2</sub>O than the  
293 Central Kalimantan Sintang Suite group for any SiO<sub>2</sub> content (Fig. 5a & g). Intrusive rocks with less  
294 than 55 wt. % SiO<sub>2</sub> have not been found in West Sarawak.

295 Like major elements, the incompatible trace element concentrations in West Sarawak Sintang  
296 intrusive rocks are coherent with diorites previously analysed from this area (Prouteau et al., 2001),  
297 having substantial enrichment in the most incompatible elements with pronounced depletions of Nb  
298 compared to MORB (Fig. 6a). This means that their trace element ratios broadly resemble volcanic  
299 arc or post-collision rocks (Supplementary Fig. 1). However, the new analyses show that the Nb  
300 depletion is accompanied by large enrichments in Pb. While these characteristics can be indicative of  
301 subduction, they can also be produced or enhanced if crust contaminates intruding magma, as

302 demonstrated for the Semporna peninsula of northeast Borneo in Sabah (Fig. 7a; Macpherson et al.,  
303 2010). Likewise, melting of a crustal source with such patterns would also generate these features.  
304 The new Kuching intrusive rock data show concentrations of Y and Yb that are similar to or slightly  
305 lower than N-MORB (Fig. 6a). We found no West Sarawak Sintang intrusive rocks showing the strong  
306 depletion of Y and heavy rare earth elements that led Prouteau et al. (2001) to identify adakites in  
307 this area. Trace element ratios support the conclusion from major element data, that these West  
308 Sarawak Sintang intrusive rocks more closely resemble the Northern and Southern Kalimantan  
309 Sintang groups than the Central Kalimantan Sintang group (Fig. 6d).

### 310 *5.1.2. Volcanic rocks*

311 Volcanic samples are rhyolites and rhyodacites with SiO<sub>2</sub> ranging from 74 to 77 wt. %, and a single  
312 trachydacite with SiO<sub>2</sub> = 61 wt. % (Supplementary Fig. 1). Major elements in TB161 are similar to  
313 West Sarawak Sintang intrusive rocks with similar SiO<sub>2</sub> contents, except for lower CaO and higher  
314 Na<sub>2</sub>O (7.87 wt. %; Fig. 5). The more silicic volcanic rocks lie on extensions of the array for West  
315 Sarawak Sintang intrusive rocks. Based on potassium contents the volcanic rocks are calc-alkaline,  
316 and they are predominantly peraluminous (Supplementary Fig. 1).

317 Normalised incompatible element patterns show slight differences from the intrusive rocks. The  
318 most incompatible elements show similar ratios with similar to slightly higher contents. However,  
319 compared to intrusive rocks these more silicic rocks display depletions of several elements that can  
320 be accommodated in phases crystallised from felsic melts (Fig. 6b). Thus, pronounced depletions in P  
321 suggest crystallisation of apatite while depletion of Sr, along with Al<sub>2</sub>O<sub>3</sub> and CaO, is consistent with  
322 plagioclase fractionation, and Zr depletion may result from zircon fractionation. Relative depletion of  
323 Ti could reflect fractionation of oxide phases or of amphibole. The mild, overall enrichment of  
324 incompatible elements with relative depletion of compatible elements is consistent with the West  
325 Sarawak Sintang volcanic rocks being more differentiated equivalents of the West Sarawak Sintang  
326 intrusive rocks. High-silica rocks with very similar trace element patterns are found in the Northern,

327 Central, and Southern groups of the Kalimantan Sintang Suite (Williams and Harahap, 1987;  
328 Harahap, 1993).

### 329 *5.2. Bau Suite*

330 Rocks from the Bau District are granodiorites and can be described as magnesian calcic and range  
331 from peraluminous or metaluminous (Supplementary Fig. 1). Based on K<sub>2</sub>O content, they are calc-  
332 alkaline (1.3 to 2.9 wt. %; Supplementary Fig. 1). SiO<sub>2</sub> contents range from 67.5 to 71.8 wt. %. This  
333 extends the range previously recognised by Prouteau et al. (2001) to slightly higher silica values,  
334 while other major elements are similar to those by Prouteau et al. (2001) except for slightly higher  
335 Al<sub>2</sub>O<sub>3</sub> in the least silicic rocks. Major elements of the Bau Suite resemble West Sarawak Sintang rocks  
336 with similar SiO<sub>2</sub> although they have slightly more elevated Al<sub>2</sub>O<sub>3</sub> and CaO. This makes the Bau Suite  
337 more similar to Kalimantan's Central Sintang group than the Northern or Southern groups (Fig. 5).

338 Compared to N-MORB, the most incompatible trace elements are the most enriched in Bau Suite  
339 rocks. For most elements, the level of enrichment gradually diminishes through to the middle rare  
340 earth elements and then remains constant or becomes progressively depleted for less incompatible  
341 elements (Fig. 6c). Superimposed upon this pattern are relative depletions in Nb, Ta, and Ti and, to a  
342 lesser extent, P along with pronounced enrichments in K and Pb and, to a lesser extent, Sr as  
343 discussed above (Fig. 6c).

344 The new analyses of the Bau Suite rocks show contents and ratios of incompatible trace elements  
345 similar to prior analyses of the Bau Suite and other adakitic rocks from the Kuching/Bau area  
346 (Prouteau et al., 2001; Fig. 7b). For both, contents of and ratios between more incompatible  
347 elements are similar to the West Sarawak Sintang intrusive rocks with similar SiO<sub>2</sub>, but the heavy  
348 rare earth elements and Y are more variable. Some resemble the West Sarawak Sintang Suite but  
349 most are relatively depleted in Y and HREE (Fig. 6c). Compared to the Kalimantan Sintang Suite, the  
350 Bau Suite most closely resembles the Central group (Fig. 6d, Fig. 7b), consistent with the conclusion  
351 drawn from major elements.

352

## 353 6. U-(Th)-Pb zircon geochronology

### 354 6.1. West Sarawak Sintang Suite

#### 355 6.1.1. Intrusive rocks

##### 356 *Sample TB63b*

357 TB63b is a granodioritic sill intruding the Kayan Sandstone at Tanjung Santubong. Zircons are usually  
358 euhedral to subhedral or anhedral. Simple internal zoning is evident in most grains. Concentric,  
359 patchy and sector zoning are rare.

360 86 U-Pb ages were obtained from 86 zircon grains (Fig. 8a). The zircon age population is  
361 predominantly Early Miocene (83 ages) with one inherited age of  $256 \pm 4$  Ma. Two Miocene ages  
362 were excluded because of high common lead. Two outliers of Miocene age were excluded from the  
363 weighted mean age calculation because of lead-loss, resulting in a unimodal population (Fig. 9a) of  
364 81 Miocene ages (98% of total Miocene ages) that cluster between 19 and 23 Ma with a weighted  
365 mean age of  $21.1 \pm 0.2$  Ma (MSWD = 3.5).

##### 366 *Sample TB58*

367 TB58 is a stock that intrudes sediments of the Silantek Formation sampled from a granodiorite  
368 boulder in a small gully from Bukit Kelambi (Klambi). Zircons are angular, with a euhedral to  
369 subhedral or anhedral shape. Elongate zircons dominate. Simple internal zoning is evident in most  
370 grains. Concentric, oscillatory, patchy and sector zoning were also observed. Zircons with inherited  
371 ages are commonly oscillatory zoned and subrounded.

372 51 U-Pb ages were obtained from 51 zircon grains (Fig. 8b). A single Miocene age was excluded  
373 because of high common lead. The population is predominantly Early Miocene (43 ages) with 7  
374 inherited zircons of Mesozoic to Permian age, ranging from 114 to 267 Ma. 7 outliers of Miocene  
375 ages (grey in Fig. 8b) have either lead-loss or inheritance, and were excluded from the weighted  
376 mean age calculation. This includes a small population composed of 5 inherited Miocene zircons at

377 around 23 Ma, leaving a unimodal population of 36 of the 43 Miocene ages (84% of the Miocene  
378 ages), which cluster between 19.4 and 21.8 Ma with a weighted mean age of  $20.3 \pm 0.2$  Ma (MSWD =  
379 3.0).

#### 380 *Sample TB33*

381 TB33 is a dyke sampled from Gunung Bawang at 300 m above sea level and close to the Serapi dyke  
382 dated by the K-Ar method as  $25.8 \pm 1.9$  Ma (Schmidtke et al., 1990). Zircons are euhedral to  
383 subhedral or anhedral. Elongate varieties are common. Simple internal zoning is evident in most  
384 grains. Concentric, patchy and sector zoning is also observed. Oscillatory zoned grains are rare.  
385 Zircons are bright to grey with darker edges in CL. Very thin light coloured, potentially magmatic,  
386 rims are observed in a few grains.

387 66 U-Pb ages were obtained from 61 zircon grains (Fig. 8c). Two ages were excluded because of  
388 partial ablation of the resin mount. The zircon population is predominantly Early Miocene (63 ages)  
389 with one inherited age of 500 Ma. Six Miocene outliers, including a small population of inherited  
390 Miocene zircons at around 24 Ma and a number of zircons affected by lead-loss, were identified and  
391 excluded from the weighted mean age calculation. The remaining Miocene population has a  
392 unimodal distribution (Fig. 9c) including 57 of the 63 (91% of all) Miocene ages, clustering between  
393 18 and 22 Ma with a weighted mean age of  $20.1 \pm 0.2$  Ma (MSWD = 2.1).

#### 394 *6.1.2. Volcanic rocks*

##### 395 *Sample TB141*

396 TB141 is a rhyolite from a lava flow exposed in a road cut near Kampung Matang in the Gunung  
397 Serapi area and contains zircons of two different varieties. The majority are elongate euhedral  
398 needle-like grains with simple internal or sector zoning, which are Miocene (see below). Other  
399 zircons are subhedral to subrounded with simple internal or oscillatory zoning which yielded  
400 inherited ages.

401 42 U-Pb ages were obtained from 41 zircon grains (Fig. 9a). Six ages were excluded because of  
402 discordance or lead-loss (not displayed in the Tera-Wasserburg diagram). The remainder are mainly  
403 Early Miocene (23 ages), with inherited zircons of Oligocene ( $33 \pm 0.5$  Ma), Cretaceous ( $66.6 \pm 0.8$   
404 Ma and  $100 \pm 1$  Ma), Triassic (216 to 240 Ma), Permian ( $271 \pm 4$  Ma) and Proterozoic (773 to 1911  
405 Ma) age. After rejection of one age, potentially affected by lead-loss, the Miocene population is  
406 bimodal. 7 Miocene ages (violet in Fig. 10a) range from 20.9 to 22.3 Ma with a weighted mean age of  
407  $21.5 \pm 0.4$  Ma (MSWD = 1.5) and are interpreted as inherited from an early phase of magmatism. The  
408 younger population includes 15 of the 23 (65% of all) Miocene clustering between 19 and 20.5 Ma  
409 with a weighted mean age of  $19.8 \pm 0.3$  Ma (MSWD = 1.3) interpreted as the eruption age.

#### 410 *Sample TB209a*

411 Sample TB209a was sampled from a rhyolite boulder field near Bukit Buwaya. Like TB141, there are  
412 two varieties of zircon from TB209a. Euhedral to subhedral elongate needle varieties have simple  
413 internal or sector zoning with bright to greyish CL imagery and are Miocene (see below). Inherited  
414 zircons are subrounded to anhedral, usually with sector or oscillatory zoning.

415 41 U-Pb ages were obtained from 38 zircon grains (Fig. 9b). Two inherited ages were excluded for  
416 failing the 10% discordance criteria and two Miocene ages were also excluded because of abundant  
417 common lead. The age population is mainly Miocene, with inherited Eocene ( $47.1 \pm 0.6$  Ma),  
418 Cretaceous (68.5 to 105 Ma), and Neoproterozoic ( $649 \pm 7$  Ma) ages. Two Miocene outliers (violet  
419 colour) were identified and are interpreted as inherited ages of c. 20.3 Ma. The remaining unimodal  
420 population (Fig. 10b) includes 25 of 27 (93% of all) Miocene ages clustering between 17.9 and 19.4  
421 Ma with a weighted mean age of  $18.6 \pm 0.2$  Ma (MSWD = 2.0).

## 422 6.2. *Bau Suite*

### 423 *Sample TB9*

424 TB9 is a micro-tonalite from the Bukit Stigang quarry southeast of Kuching (Kota Samarahan).  
425 Euhedral, elongated zircons with simple or concentric zoning and greyish CL imagery are common.

426 25 U-Pb ages were obtained from 22 zircons (Fig. 9c). Two inherited ages were excluded for failing  
427 the 10% discordance criteria. The youngest grain of 5 Ma is interpreted to be affected by lead-loss  
428 and was also excluded. Of the valid ages 19 are Miocene, with three Miocene outliers either affected  
429 by lead-loss or inheritance (marked in grey) and excluded from the weighted mean age calculation,  
430 leaving a unimodal population which includes 16 of 19 (84% of all) Miocene ages which cluster  
431 between 12.6 and 14.5 Ma with a weighted mean age of  $14.1 \pm 0.1$  Ma (MSWD = 0.5).

#### 432 *Sample TB61*

433 Sample TB61 is a micro-granodiorite collected from the Bukit Stapok quarry in Batu Kawa near  
434 Kuching that contains euhedral, elongate zircons with simple or oscillatory zoning. Larger zircons are  
435 anhedral, can be easily distinguished from elongate varieties, and are inherited. 10 U-Pb ages were  
436 obtained from the sample (Fig. 9d). Two inherited ages were excluded after failing the 10%  
437 discordance criteria and one Miocene age was excluded because of abundant common lead. The  
438 sample has one concordant inherited Proterozoic age around 850 Ma. The youngest population of  
439 the sample ranges from 4.6 to 18.5 Ma (Fig. 9d). The youngest grain of 4.6 Ma is interpreted to be  
440 affected by lead-loss. Three analyses lie close to 12 Ma (and the excluded Miocene age with  
441 abundant common lead as well) and the age is interpreted as a crystallisation age with a weighted  
442 mean age of  $12.4 \pm 0.9$  Ma (MSWD = 1.4). Two ages of 15 and 18.5 Ma are interpreted as inherited.

## 443 **7. Discussion**

### 444 *7.1. Age of Neogene magmatism*

#### 445 *7.1.1. West Sarawak Sintang Suite*

446 Our U-Pb dating of zircons in volcanic and intrusive rocks from West Sarawak yielded a restricted  
447 range of ages (Fig. 10a), suggesting relatively short-lived Miocene magmatic episodes. The intrusive  
448 rocks gave weighted mean ages of 20.1 to 21.1 Ma (Tab. 2; Fig. 10a). We interpret the slightly older,  
449 inherited ages of 22 to 24 Ma (n = 7) as recording earlier magmatic activity during the latest  
450 Oligocene to earliest Miocene. We obtained a U-Pb age of  $20.1 \pm 0.2$  Ma for the Bawang dyke

451 (TB33), which is only a few metres away from the Serapi dyke previously dated by the K-Ar method  
452 as  $25.8 \pm 1.9$  Ma (Schmidtke et al., 1990). Both dykes are likely to be part of the same magmatic  
453 phase and we suggest the U-Pb age is more accurate.

454 Since West Sarawak Sintang volcanic rocks gave ages of  $18.6 \pm 0.2$  Ma and  $19.8 \pm 0.3$  Ma (Tab. 2; Fig.  
455 10a), which are within analytical uncertainty of the intrusive rocks, we interpret both to be part of  
456 the same suite. This is consistent with the geochemical data which indicate that the volcanic rocks  
457 are silicic differentiates of the intrusive magmas. It is notable that both volcanic samples contain  
458 inherited zircons with ages ranging from 19.8 to 22.7 Ma, which resemble the ages of the intrusive  
459 rocks (Fig. 10a). This is further evidence for pulsed early Miocene magmatic activity. Thus, we  
460 suggest the West Sarawak Sintang Suite records a period of magmatism from c. 24 to 18.5 Ma during  
461 which there were potentially three pulses. A tuff layer in the Temburong Formation on Labuan (Fig.  
462 2) was recently dated as c.  $19.5 \pm 0.1$  Ma (S. Burley, pers. comm., 2018). The age is indistinguishable  
463 from the Sintang Suite, and the tuff could be an airfall record of the same activity, 650 km from the  
464 Sintang rocks.

#### 465 7.1.2. *Bau Suite*

466 The youngest magmatic activity we dated in West Sarawak is the 12.4 to 14.1 Ma Bau Suite (Tab. 2;  
467 Fig. 10a), with ages similar to K-Ar dates from Bau quartz-porphyrines (10 to 12 Ma; JICA, 1985), and  
468 K-Ar dates of adakitic microtonalites in Bau and south of Kuching (6.4 to 11.6 Ma; Prouteau et al.,  
469 2001). The range of our U-Pb ages is narrower than those of Prouteau et al. (2001), but each of our  
470 samples contain a younger zircon of c. 5 Ma showing lead loss, which suggest Pliocene thermal  
471 effects of magmatism or hydrothermal activity. Basaltic magmatism at c. 5 Ma has been reported  
472 from Mount Niut in Kalimantan (Harahap, 1994), only 30 km south-southwest of the Bau intrusive  
473 field (Fig. 2). Pliocene thermal activity could have affected Miocene whole rock ages obtained by the  
474 K-Ar method.

475 We conclude that the Bau episode was confined to a relatively short interval in the Middle Miocene,  
476 which may be contemporaneous with the Kuching adakites reported by Prouteau et al. (2001).  
477 Ramkumar et al. (2018) obtained U-Pb ages of 11.44 to 11.76 Ma (n = 3), indistinguishable from our  
478 younger Bau age, for a tephra layer in coal beds near Mukah, approximately 300 km northeast of  
479 Bau (Fig. 2). This tephra layer is around 6 cm thick, contains no large pyroclastic fragments, and  
480 contains non-vesicular glass along with clasts of non-juvenile origin, which Ramkumar et al. (2018)  
481 interpreted as reflecting the distal deposit of a large volcanic event. Geochemical characterisation of  
482 the tephra is complicated by deposition of contemporaneous sediment and then by significant post-  
483 depositional alteration. Some trace element ratios of Mukah tephra resemble Bau, although others  
484 are more similar to the West Sarawak Sintang Suite, and all have a strong alteration overprint on the  
485 most mobile elements (Ramkumar et al., 2018). The chemistry of this tephra layer is, however, not  
486 inconsistent with an origin from Bau. Potential eruptive products near Bau town include a 1 x 2 km  
487 dome of rhyodacite flow breccia at Gunung Sirenggok (Schuh, 1993). Such silicic magmas are often  
488 associated with highly explosive eruptions that can disperse large ash falls up to hundreds of  
489 kilometres from their source. Furthermore, the Bau granites were emplaced into Mesozoic  
490 limestones (Schuh, 1993), which could have enhanced the volatile content, and therefore the  
491 explosivity, of magma that reached the surface. Schuh (1993) documents several instances of  
492 brecciation of Bau intrusive bodies, which could reflect syn-emplacement magmatic activity or late-  
493 stage mineralisation.

494 The main phase of magmatism at Bau is Middle Miocene. We suggest this was part of more  
495 widespread igneous activity, forming adakitic stocks south of Kuching (Prouteau et al., 2001) and  
496 explosive volcanism that produced widespread blankets of ash towards the northeast (Ramkumar et  
497 al., 2018). A single, slightly older, zircon age of c. 19 Ma in TB61, indistinguishable from the age of  
498 West Sarawak Sintang rocks (Fig. 10a) suggests Early Miocene magmatism in the Bau area.

499

## 500        *7.2. Implications of inherited ages*

501    The West Sarawak Sintang Suite volcanic rocks contain abundant inherited Cenozoic, Cretaceous,  
502    Permian-Triassic, and Proterozoic zircons (Fig. 10b). Although the intrusive rocks and Bau Suite  
503    contain fewer inherited zircons, their ages are similar to those in the volcanic rocks. Two inherited  
504    zircons of Oligocene to Eocene age indicate activity in West Sarawak at a similar time to K-Ar ages  
505    for NW Kalimantan (Pieters et al., 1987; Bladon et al., 1989). Late Cretaceous inherited ages (c. 66 to  
506    80 Ma) resemble those from Upper Cretaceous intrusions in West Sarawak (Kirk, 1968; Hennig et al.,  
507    2017), and in NW Kalimantan (Williams et al., 1988). The peak in Cretaceous inherited zircon ages  
508    between 85 to 100 Ma coincides with that of the Schwaner Mountains (Haile et al., 1977; Williams et  
509    al., 1988; van Hattum et al., 2013; Davies et al., 2014; Hennig et al., 2017). Triassic inherited zircon  
510    ages resemble the Triassic Sundaland part of West Sarawak (Breitfeld et al., 2017) and in the  
511    Northwest Schwaner Zone (Hennig et al., 2017). Precambrian inherited zircons show a distribution  
512    similar to the Pedawan Formation (Breitfeld et al., 2017) and, although low in number, could  
513    indicate either re-melting of Pedawan Formation or re-melting of source rocks of the Pedawan  
514    Formation. The inherited zircons provide clear evidence of significant crustal input to both the  
515    Sintang and Bau magmatism.

## 516        *7.3. Magma source*

517    The absence of active subduction to the west of the West Baram Line at the time of emplacement of  
518    the Bau, the West Sintang-Sarawak, and Kalimantan Sintang suites (Section 2) eliminates fractional  
519    crystallisation of arc magma as a possible source for these suites (Macpherson et al., 2006). Any  
520    petrogenetic model for these suites must also reconcile the restricted contrasts in composition  
521    between the adakitic and non-adakitic rocks of western Sarawak, and recognise the presence of  
522    some non-adakitic rocks amongst the Bau Suite. Other than the depletion of heavy rare earth (and  
523    associated) elements in the adakitic rocks there are few differences between West Sarawak Sintang  
524    and Bau suites, after accounting for crystallisation of minor phases e.g. apatite and oxides (Fig. 6).  
525    This leads us to conclude that Bau and West Sarawak Sintang rocks are, ultimately, derived from

526 similar sources. Furthermore, the non-HREE-depleted, dioritic West Sarawak Sintang Suite rocks  
527 resemble Kalimantan's Northern and Southern Sintang groups, while the HREE-depleted Bau rocks  
528 more closely resemble the Central Sintang group from Kalimantan (Figs. 5 to 7). This suggests that  
529 the source(s) of these magmas were present throughout large parts of western Borneo from the late  
530 Paleogene until the middle Neogene.

531 To explain the adakitic character of the Bau Suite in the absence of active subduction, Prouteau et al.  
532 (2001) proposed that a previously subducted piece of oceanic lithosphere had stalled in the mantle  
533 and melted. Neither the seismic tomography images available at the time (Rangin et al., 1999) nor  
534 since (Hall and Spakman, 2015) have identified an anomaly at suitable depths in the mantle  
535 suggesting such a slab.

536 The tomographic observations are insufficient to disprove the absence of a slab, but we note that  
537 the compositions of Bau Suite rocks show several differences from experimentally-generated melts  
538 of hydrated basalt at mantle pressures (Winther and Newton 1991; Sen and Dunn, 1994; Rapp and  
539 Watson, 1995). At any particular SiO<sub>2</sub> content, Bau Suite adakitic rocks are displaced to lower Na<sub>2</sub>O,  
540 TiO<sub>2</sub>, and Al<sub>2</sub>O<sub>3</sub>, and to higher MgO than predicted by experiments (Fig. 5). The deviation from  
541 experimental slab melt compositions cannot be due to interaction between slab melts and mantle  
542 (Kay, 1978; Martin, 1999; Martin et al., 2005; Yogodzinski et al., 2001) since the Borneo rocks do not  
543 display the systematic decrease in the aluminium saturation index (molar [Al / Ca + K + Na]) with  
544 only a small change in SiO<sub>2</sub> that Rapp et al. (1999) have showed would result from such a process  
545 (Fig. 5). In all respects, the major element compositions of the Bau Suite behave more coherently  
546 with the non-adakitic West Sarawak Sintang Suite than with the experimental slab melts. For trace  
547 elements the two suites show differences only in the HREEs and Y, with all West Sarawak Sintang  
548 and some Bau rocks showing no trace element adakitic signature (Fig. 6).

549 In view of these observations, we conclude that both the adakitic and non-adakitic rocks of Bau and  
550 Sintang were derived from similar sources. Although it is reasonable to conclude that this was a

551 basaltic source, production of non-adakitic magma from a basaltic composition requires melting at  
552 pressures of less than 10 kbar which is not feasible for the depth of any subducted slab that may be  
553 postulated beneath Borneo. Therefore, we conclude that the magmatism of West Sarawak and, by  
554 extension, the main Sintang Suite of Kalimantan, do not support the model of a stalled slab beneath  
555 Borneo.

### 556 *7.3.1. Crustal melting at low pressure*

557 The involvement of crust in the genesis of the compositional intermediate magmatism is indicated  
558 by the zircons with inherited ages in all suites (Fig. 10b). Major element compositions of Sarawak  
559 igneous rocks are well approximated by melting experiments conducted at pressures below 7 kbar  
560 where dehydration-melting and water saturated-melting of amphibolites yield intermediate  
561 composition melts with  $\text{Al}_2\text{O}_3$ ,  $\text{TiO}_2$ , and  $\text{Na}_2\text{O}$  contents that are lower than those from experiments  
562 above 10 kbar (Beard and Lofgren, 1991). These lower pressure, particularly dehydration,  
563 experiments also produce intermediate composition melts with MgO contents more elevated than  
564 from high pressure melting, although not quite to the level of the Sarawak rocks. Thus, melting of  
565 hydrated basalt in the mid- to deep-crust below Borneo could produce much of the major element  
566 variation character of non-adakitic rocks of West Sarawak, and in the Northern and Southern groups  
567 of the Kalimantan Sintang Suite. Such magmas would not have significant depletions in the heavy  
568 rare earth elements, and therefore would not appear adakitic, because melting occurred at  
569 pressures below those at which garnet is stable.

### 570 *7.3.2. Crustal melting at high pressure*

571 We have discounted slab melting for the Sintang and Sarawak adakitic rocks principally because (i)  
572 they show many similarities to contemporaneous non-adakitic rocks which lack heavy rare earth  
573 element depletion, and (ii) they show negligible sign of having interacted with the mantle. These  
574 factors do not exclude melting of hydrated basalt with garnet present at greater depths in the crust.  
575 Such melting would produce an adakitic signature (strong depletion of HREE and Y) while having

576 negligible effect on other trace elements (Fig. 6). Furthermore, because melting occurred in the  
577 crust, the intermediate to evolved composition magma would not interact with the mantle (Fig. 11a  
578 and b). High silica magmas would equate to low degrees of melting, and as the degree of melting  
579 increase  $\text{SiO}_2$  would decrease (Rapp and Watson, 1995). However, on its own, this mechanism has  
580 two problems. First, for any realistic  $\text{SiO}_2$  content the lowest MgO contents of the Sintang and Bau  
581 Suite rocks are at the upper range of even the low pressure melting experiments (Beard and Lofgren,  
582 1991). Second, the presence of mafic rocks, including andesitic compositions in the West Sarawak  
583 Sintang Suite and basaltic compositions in the Kalimantan Sintang Suite (Fig. 5), would require very  
584 high degrees of melting, in excess of 50 % at temperatures well above  $1050^\circ\text{C}$  (Rapp and Watson,  
585 1995). These issues can be resolved by considering the origin of the most mafic Sintang Suite rocks  
586 ( $\text{MgO} > 3 \text{ wt. \%}$  and  $\text{SiO}_2 < 58 \text{ wt. \%}$ ).

### 587 *7.3.3. Crustal melting with a contemporaneous mafic input*

588 Mafic rocks from the Sintang Suite are different to the intermediate and evolved rocks. The mafic  
589 rocks have basaltic to low-silica andesitic compositions (Williams and Harahap, 1987; Harahap, 1993;  
590 Heryanto et al., 1993; Prouteau et al., 2001) in which silica correlates positively with  $\text{Al}_2\text{O}_3$ ,  $\text{K}_2\text{O}$  and  
591  $\text{Na}_2\text{O}$ , and shows a strong, negative correlation with MgO (Fig. 5). These mafic rocks show less  
592 extreme ratios of fluid-mobile to non-mobile incompatible trace elements and less marked depletion  
593 of the moderately incompatible elements (Nd to Y) than the more silicic rocks leading to smoother  
594 normalised trace element patterns (Fig. 7a). The mafic rocks also tend to have steeper patterns for  
595 the heavy rare earth elements which, for basaltic rocks, is likely to indicate melting of garnet  
596 peridotite. Most show notable depletion in Nb, which might be interpreted as indicating a  
597 subduction setting. However, HFSE depletion can also be produced by crustal contamination even in  
598 relatively mafic melts (Thompson et al., 1983), and this has been proposed for basalts from the  
599 Semporna Peninsula in Sabah, NE Borneo (Macpherson et al., 2010). The major and trace element  
600 compositions of mafic Sintang rocks resemble basalts from Semporna (Fig. 7a), and we therefore  
601 interpret the mafic members of the Sintang Suite to be mantle-derived magma that has been

602 contaminated by crust. The presence of such rocks among the Sintang Suite has two important  
603 implications. First, mantle melting was contemporaneous with the emplacement of intermediate to  
604 evolved magma that makes up the bulk of the Neogene activity. Second, those mafic magmas  
605 interacted with the crust, both bringing extra heat into, and causing sufficient localised melting of,  
606 those rocks to allow contamination to occur.

607 Projections from compositions of intermediate and evolved West Sarawak and Kalimantan Sintang  
608 rocks toward lower  $\text{SiO}_2$  tend towards the more evolved end of the array of mafic rocks for all major  
609 elements (Fig. 5). This is particularly evident for  $\text{Al}_2\text{O}_3$ ,  $\text{TiO}_2$ , and  $\text{Na}_2\text{O}$ , where the Borneo rocks  
610 diverge from the fields for high pressure melting experiments of hydrated basalt towards lower  
611 concentrations, and even more striking for the displacement to relatively high MgO contents (Fig.  
612 5d). We propose that, rather than recording variable degrees of partial melting of hydrated basalt,  
613 the wide range of silica contents observed in the intermediate and evolved rocks from West Sarawak  
614 and Kalimantan reflects mixing of mantle-derived and crustal-derived magmas. The low-silica end of  
615 the array is directed towards input of mantle melts, which must have experienced some  
616 differentiation to produce the range from basalt through to low-silica andesite. This differentiation  
617 also involved interaction with crust to lower the Nb contents. The high-silica end of the West  
618 Sarawak and Kalimantan Sintang array is directed towards crustal melts, which appear to represent a  
619 restricted range of very high-silica compositions, in turn suggesting relatively low degrees of partial  
620 melting of hydrated basaltic crust. However, some of the scatter, particularly of Central Sintang  
621 rocks from Kalimantan, may reflect higher degrees of melting and/or involvement of more deeply  
622 derived crustal melts. The depth of melting would determine the strength of the adakitic signature  
623 i.e. the extent of the HREE-depletion, in the crustal contribution to each melt batch. Thus, for  
624 example, it is not paradoxical that intermediate rocks of the Central Sintang group have more  
625 elevated Sr/Y than the more silicic Bau Suite. This is simply a function of the crustal component in  
626 the Central Sintang magmas being derived from greater depth than the Bau Suite, but that these  
627 then mixed with a greater volume of mantle-derived mafic magma than occurred at Bau.

628 We conclude that the intermediate to evolved rocks from West Sarawak and Kalimantan are  
629 mixtures of mafic magma generated in the mantle with crustal melt derived from basalt that was  
630 originally hydrated or became so through subsequent metamorphism (Johnson et al., 1978; Smith et  
631 al., 1979; Rogers et al., 1985; Macpherson et al., 2006, 2010; Macpherson, 2008). As mixtures, it is  
632 difficult to place firm constraints on the depth at which crust melted because none of the intrusive  
633 rocks represent pure crustal melt. The presence of adakitic chemistry does indicate that zone of  
634 crustal melting extends across the garnet-in boundary.

#### 635 *7.3.4. Source of the crustal melt*

636 There are various potential sources of hydrated basaltic rock in the Borneo crust. The Bau Suite  
637 intrudes crust that contains Triassic arc rocks (e.g. Serian Volcanics, Jagoi Granodiorite), attesting to  
638 prior arc activity which affected that lithospheric block (Schuh, 1993; Breiffeld et al., 2017). This  
639 Triassic block does not extend east across the whole area of the Sintang Suite (Breiffeld et al., 2017;  
640 Hennig et al., 2017), but the Schwaner Mountains granitoids represent a long-lived Mesozoic  
641 convergent margin (Williams et al., 1988; Davies et al., 2014; Hennig et al., 2017; Hall and Breiffeld,  
642 2017 and references therein) at which basaltic magma could have been emplaced into the  
643 arc/forearc region that is now occupied by the Melawi and Ketungau basins, which host most  
644 Sintang intrusions (Figs. 2 and 11a). Alternatively, these basins may be partly underlain by accreted  
645 continental crust intruded by basaltic magmas and fragments of oceanic crust (e.g. Haile et al., 1994;  
646 Moss, 1998; Breiffeld et al., 2017). In either case there is scope for the Borneo crust to contain  
647 hydrated basaltic sources (Fig. 11a). The melanges observed at the margins of the Melawi and  
648 Ketungau basins are further evidence of the presence of basaltic rocks and the significant  
649 deformation they have experienced (Tan, 1979; Williams et al., 1988; Haile et al., 1994). Melting of  
650 such basalts could produce the felsic components of the Neogene intrusives in western Borneo by  
651 melting at higher pressures to produce adakitic magma, and at lower pressures to produce non-  
652 adakitic magma (Fig. 11a and b).

653        *7.4. Cause of magmatism*

654        We have discussed how the crustal thickening (Williams and Harahap, 1987) and/or melting of  
655        subducted crust (Prouteau et al., 2001) that have previously been proposed for the Sintang and Bau  
656        suites are inconsistent with the geology of Borneo (Section 2). Instead, we have identified that  
657        emplacement of these suites was accompanied by contemporaneous, mafic, mantle-derived  
658        magmatism. This magmatism, or the increased heatflow associated with it, was most probably  
659        responsible for causing crustal melting.

660        Roberts et al. (2018) suggested that the mantle beneath Borneo is hotter than ambient mantle but a  
661        hotspot origin can be discounted for the West Sarawak and Kalimantan Sintang magmatism.  
662        Postulated plumes with similar dimensions to the Sintang province tend to be associated with  
663        extensive, tholeiitic flood basalt magmatism and/or formation of large-scale batholiths and  
664        volcanoes (Coffin and Eldholm, 1994; Bryan and Ernst, 2008). In contrast, the Sintang and Bau suites  
665        form only isolated, and predominantly felsic, stocks, dykes, sills and rare lavas. Furthermore, hotspot  
666        models allow for a broadly distributed “plume head” stage giving way to more spatially-restricted  
667        magmatism, usually showing an age progression in a particular direction. However, the post-  
668        Miocene, mafic magmatism on Borneo – from Niut in the west to Semporna in the east – has an  
669        even broader geographic range than the Oligo-Miocene products (Fig. 2). We consider it highly  
670        unlikely that a hotspot could produce the widely dispersed, episodic Cenozoic magmatism in Borneo.

671        A west to east younging of Oligo-Miocene magmatism of western and central Borneo has been  
672        proposed by several studies (Kirk, 1968; Williams and Harahap, 1987; Schmidtke et al., 1990; Moss et  
673        al., 1998), but our new geochronological data suggest that this is not the case. First, the youngest  
674        part of this magmatism occurred in the west of Sarawak at Bau and around Kuching. Second, at Bau  
675        there are older magmatic zircons, similar in age to the West Sarawak Sintang intrusive rocks. Third,  
676        the West Sarawak Sintang intrusive rocks also show evidence of pulsed magmatism at individual  
677        sites, albeit over shorter timescales than previously proposed for the magmatic evolution of the

678 whole area (Fig. 10a). Fourth, our U-Pb ages suggest that previous K-Ar data may have  
679 overestimated the spread of ages for magmatism (cf. Bawang and Serapi dykes). Fifth, U-Pb dating of  
680 Sintang-type magmatism elsewhere in Borneo has obtained ages of 19 to 20 Ma for igneous rocks in  
681 the Kelian district (Setiabudi et al., 2007; Davies et al., 2008). Although Kelian is about 500 km from  
682 Kuching (Fig. 2) the similarity of high-precision radiometric ages is striking and suggest a widespread,  
683 short-lived, Early Miocene magmatic episode across much of central Borneo.

#### 684 *7.4.1. Extension or transtension*

685 The distribution of magmatism in western Sarawak appears to represent repeated exploitation of  
686 particular sites in the lithosphere by multiple phases of magmatism. Williams & Harahap (1987)  
687 proposed significant crustal control on the intrusion of the Sintang Suite in west Kalimantan, where  
688 they noted both that intrusions were aligned with one another and that larger intrusions tended to  
689 be associated with the central parts of basins. Similarly, the overall trend of the West Sarawak  
690 Sintang Suite suggests reactivation of WNW-ESE-directed faults of similar orientation to the Lupar  
691 Line (Fig. 2 and Fig. 11b). Schuh (1993) attributed the Bau Suite intrusions to one or two deep  
692 batholiths intruded along an existing, ENE-striking crustal weakness which he interpreted as a  
693 transtensional system. Stocks from this intrusion then intruded to shallower levels where an active,  
694 NNE-striking, regional, transtensional fault system intersected other existing structures in the crust.  
695 Thus, the actual emplacement of individual intrusive bodies now seen at the surface was controlled  
696 locally at relatively shallow scale. Evidence that this Bau trend has been a site of magmatism  
697 throughout the Neogene comes from the inherited 19 Ma zircon in TB61, and the resetting of some  
698 Bau zircon ages to the age of younger (c. 5 Ma), Niut magmatism, which lies along the same NNE-  
699 trending fault system (Harahap, 1994).

700 Association of magmatism with transtensional settings, similar to the Lupar Line fault system, is  
701 known from modern and ancient locations such as Death Valley, the Red River Fault, and the  
702 Midland Valley of Scotland (e.g. Calzia and Ramo, 2000; Monaghan and Parrish, 2006; Hussein et al.,

703 2011). Crustal thinning associated with tension allows the mantle to upwell and, hence, melt  
704 (McKenzie and Bickle, 1988).

705 The timing of extension and crustal thinning in Borneo is best constrained by the depocentre of the  
706 Kuching Supergroup basins, which Breitfeld et al. (2018) interpreted as strike-slip basins. A  
707 transtensional component to this system could be indicated by the basement pop-up structures that  
708 bound these sedimentary basins. However, the Maastrichtian to Eocene ages of these deposits  
709 significantly pre-date the Oligo-Miocene magmatism studied in this paper (Fig. 10a). The Neogene  
710 igneous rocks are not deformed and indicate that significant movement along these faults had  
711 stopped prior to magma emplacement. Van Leeuwen et al. (1990) and Douth (1992) proposed  
712 emplacement of the Sintang Suite in Kalimantan after folding of Eocene/Oligocene sediments, and  
713 Moss et al. (1998) concluded that they were emplaced immediately after a phase of deformation at  
714 about c. 25 Ma. Breitfeld et al. (2017) presented  $^{40}\text{Ar}/^{39}\text{Ar}$  ages from white micas in schists south of  
715 Kuching, which can be interpreted as evidence of deformation in West Sarawak at c. 25 to 30 Ma.  
716 Therefore, the magmatism is unlikely to be associated with large scale active extension or  
717 transtension of the Borneo crust.

#### 718 *7.4.2. Lithospheric thinspots and plate motion*

719 Basaltic magmatism can be generated by mantle melting beneath lithospheric thin spots, even in the  
720 absence of active extension. As long as there is a mechanism for mantle to rise into, and through,  
721 those thin spots, then melting can occur (King and Anderson, 1998). A number of studies have  
722 recently advocated plate motion as such a mechanism to allow such upwelling (Macpherson et al.,  
723 2010; Conrad et al., 2010, 2011; Ekici et al., 2012, 2014).

724 The lithosphere of Borneo is thinner than adjacent portions of the Sunda Shelf (Roberts et al., 2018)  
725 and the extensive Kuching depocentre implies that a broad swathe of crust between the Lupar Line  
726 and the Schwaner Mountains experienced substantial crustal thinning from the Cretaceous until the  
727 mid-Cenozoic (Eocene-Oligocene) (Fig. 11a). Thermal relaxation times mean that such thin spots

728 would persist for the few million years until, at least, the Late Oligocene. Thus, any subsequent  
729 rotation or translation of Borneo relative to the underlying mantle (Hall et al. 2008; Hall and  
730 Spakman, 2015) could have caused mantle upwelling and melting where the thinning had been  
731 greatest. It is possible that the Lupar Line and related structures might have been reactivated at the  
732 time of magma emplacement to enhance the potential for upwelling, although there is no evidence  
733 to support this from the sedimentary record or deformation of the Oligo-Miocene intrusives rocks.  
734 The structural fabric of the basement could, however, have provided conduits for magma transport.  
735 This is evident in the tectono-magmatic relationships at Bau (Schuh, 1993) but is also seen in  
736 alignment of stocks in other areas of the Sintang Suite (Williams and Harahap, 1987). The resorbed,  
737 variably deformed quartz crystals found in the Bau granitoids would be consistent with assimilation  
738 of vein deposits contained in such basement fault networks.

#### 739 *7.5. Adakites without subduction*

740 Their presence in continental collision zones with substantially thickened crust should provide prima  
741 facie evidence that not all magmatic rocks with adakitic chemistry can be treated as evidence of slab  
742 melting (Chung et al., 2003; Hou et al., 2004; Guo et al., 2007). Outside collision zones, the sources  
743 of adakitic magmatism are more controversial, but we have noted the absence of evidence for  
744 subduction in western Borneo for several tens of millions of years before the Sintang and Bau  
745 magmas were emplaced. Furthermore, the petrogenetic model most consistent with their  
746 composition does not support or require a subducted slab. Instead, melting of hydrous basaltic rock  
747 in the lithosphere of Borneo is the most probable cause of these rocks. Our findings extend the  
748 range of known non-subduction occurrences of adakite emplacement to a continental block that has  
749 not experienced significant, prior or contemporaneous crustal thickening.

750 Borneo is not the first non-collisional location where adakitic rocks have been documented with an  
751 absence of contemporaneous subduction (Johnson et al., 1978; Smith et al., 1979; Rogers et al.,  
752 1985; Sajona et al., 2000). The cause of magmatism in these other settings has been difficult to

753 ascertain due to subduction ceasing only recently before adakite emplacement and the potential for  
754 remnants of subducted oceanic lithosphere in the subjacent mantle (Sajona et al., 2000; Haschke  
755 and Ben-Avraham, 2005). Our findings for Borneo suggest that, rather than considering the  
756 subducted plate, melting of the upper plate should be considered as a possible source for such  
757 adakites. In each of these cases, adakitic magmas were emplaced into tectonically active blocks and  
758 in several cases were accompanied by basaltic magmatism. Therefore, Borneo may provide a better  
759 analogue for formation of those adakites than examples found in active subduction zones.

760 These conclusions indicate that adakitic chemistry alone should not be used as a direct proxy for slab  
761 melting, either in modern or ancient subduction zones. In the case of Borneo, hydrated basaltic  
762 rocks were emplaced and then remained undisturbed for many tens of millions of years, if produced  
763 by the Schwaner Mountain margin, or even hundreds of millions of years, if produced by the Triassic  
764 margin that generated the Serian Volcanics and the Jagoi Granodiorite. Thus, while it is reasonable  
765 to infer that subduction produced the hydrated, mafic rocks in the crust of Borneo from which the  
766 adakitic signature was derived, this required no more melting of a subducted slab than has been  
767 inferred to produce non-adakitic arc tholeiites and andesites (Macpherson et al., 2006; Plank et al.,  
768 2009; Bouilhol et al., 2015). Furthermore, for any location, it is not possible to conclude that the  
769 emplacement of such hydrous, mafic sources was contemporaneous with generation of the adakites  
770 themselves, without considering the prior history of the margin. Similarly, the presence of adakitic  
771 magma or rocks in modern subduction zones should not be taken as unequivocal evidence that  
772 current slabs are unusually hot. Our findings from Borneo suggest that remelting of hydrous, mafic  
773 rock produced during an earlier stage of the same margin or during the earlier history of the  
774 overriding plate should also be considered (Macpherson et al., 2006).

## 775 **Conclusions**

- 776 1. Neogene magmatism in West Sarawak produced the Lower Miocene West Sarawak Sintang  
777 Suite with ages of c. 19 to 21 Ma and the Middle Miocene Bau Suite with ages of c. 12 to 14

778 Ma (that could extent into the early Late Miocene). Inherited zircons in the West Sarawak  
779 Sintang Suite suggest magmatism was active by c. 24 Ma.

780 2. The Neogene magmatism was not related to active subduction. Geochemistry shows an  
781 adakite character for the Bau Suite while the Sintang Suite samples plot predominantly  
782 outside the adakite field. The latter appear to be part of a broader magmatic suite in west  
783 and central Borneo that does include other instances of adakitic rocks. The geochemical  
784 character of both suites is consistent with remelting of hydrous mafic rocks in the  
785 lithosphere of Borneo that were emplaced as arc basalt tens or hundreds of millions of years  
786 previously. Melting across a range of depths, from the mid- to deep-crust and the shallow  
787 lithospheric mantle, produced the range of geochemical compositions observed in the  
788 Sintang and Bau Suites.

789 3. The Neogene magmatism of west Kalimantan included a mafic component bearing within-  
790 plate trace element signatures. The mechanisms that generated this magmatism could have  
791 provided the heat to re-melt the crust, which yielded the intermediate and evolved intrusive  
792 rocks of the Sintang and Bau suites.

793 4. Production of the intraplate magmatism was the result of mantle upwelling into lithospheric  
794 thinspots. These may have been relicts from the extension which formed the Melawi and  
795 Ketungau basins and/or products of contemporaneous extension/transension. In the  
796 absence of strong evidence for the latter, upwelling into thin spots as the plate migrated is  
797 most likely to have produced the intraplate magma.

798 5. Inherited zircons within the samples are consistent with the ancient basement of Borneo  
799 playing a role in the petrogenesis of the Neogene magmatic suite of western Borneo.

800

801 **Acknowledgements**

802 This project was funded by the SE Asia Research Group of Royal Holloway University of London,  
803 which is supported by a consortium of oil companies. The Economic Planning Unit and the State  
804 Planning Unit of Malaysia made the fieldwork possible. The Mineral and Geoscience Department  
805 Malaysia, Sarawak assisted in the field, especially in person of Thomson Galin who was a great help  
806 in and off the field, and with the logistics. Richard Mani Banda is especially mentioned for his help to  
807 make this fieldwork possible. Menzies Mining is greatly thanked for providing the Bau region  
808 samples and Kai Kim Chiang for processing those that added valuable information on the Bau Suite.  
809 We thank Martin Rittner and Andy Carter (UCL/Birkbeck College) for help and support at the LA-ICP-  
810 MS facility, Christina Manning (Royal Holloway University) for assistance and data reduction of the  
811 geochemical analyses, and Andy Beard (UCL/Birkbeck College) and Dominique Tanner (University of  
812 Wollongong) for help with cathodoluminescence imaging of zircons. Andrew Kerr for editorial help  
813 and two anonymous reviewers are thanked for comments on the manuscript.

814

#### 815 **Figure Captions**

816 Fig. 1: Tectonic provinces of NW Borneo (modified after Haile, 1974; Hennig et al., 2017). The red  
817 frame shows the outline of Sintang Suite. The West Borneo basement (Triassic Sundaland) underlies  
818 also the western part of the Kuching Zone.

819 Fig. 2: Cenozoic magmatism in Borneo. Grey shaded area shows the outline of the Neogene igneous  
820 rocks. Distribution and ages from Kirk (1968), Williams and Harahap (1987), Pieters et al. (1987), van  
821 de Weerd et al. (1987), Setiawan and Le Bel (1987), Bladon et al. (1989), van Leeuwen et al. (1990),  
822 Heng (1992), Moss et al. (1998), Prouteau et al. (1996, 2001), Hutchison (2010) and Cullen et al.  
823 (2013).

824 Fig. 3: Uppermost Cretaceous to Cenozoic igneous rocks of West Sarawak with sample locations of  
825 the West Sarawak Sintang Suite and the Bau Suite. Map is based on fieldwork observations and on  
826 the geological map of Liechti et al., (1960), Heng (1992) and Hutchison (2005). Samples in bold and  
827 underlined are dated by U-Pb zircon geochronology. (Exact location of BYG8 is not known).

828 Fig. 4: Field photographs and thin section photomicrographs of Neogene igneous rocks in West  
829 Sarawak. a) Granodiorite sill at the northern tip of Tanjung Santubong intruding Paleocene  
830 sediments of the Kayan Sandstone. b) Rhyolite/rhyodacite exposure north of Gunung Serapi. c)  
831 Columnar jointed micro-granodiorite dyke of Gunung Bawang. d) Zoomed in of rhyolite lava. e)  
832 Abundant plagioclase needles and crystals with xenomorphic biotites (crossed polars; TB58). f)  
833 Epidote pseudomorph after amphibole (plane polars; TB148a). g) Monocrystalline undulose volcanic  
834 quartz with embayments and inclusions (crossed polars; TB18). h) Alkali feldspar phenocryst with  
835 twinning and sericite alteration (crossed polars; TB18). i) Intergrowth of plagioclase phenocrysts  
836 (crossed polars; TB209a). j) Subhedral clinopyroxene phenocryst (plane polars; TB161). k) Subhedral  
837 plagioclase phenocryst (crossed polars; TB9). l) Biotite with alteration corona, plagioclase and quartz  
838 phenocrysts in quartz-sericite matrix (plane polars; TB61). m) Highly rounded quartz grain,  
839 plagioclase and hornblende phenocryst (crossed polars; BYG12). (Bt = biotite, Plg = plagioclase, Ep =  
840 epidote, Am = amphibole, Qv = volcanic quartz, Kfs = alkali feldspar, Cpx = clinopyroxene, Ser =  
841 sericite, Hbl = hornblende).

842 Fig. 5: Major element variations in igneous rocks from Bau and Kuching from this work and  
843 compared with previously published data for these locations (P; Prouteau et al., 2001). Sintang Suite  
844 from northwest Kalimantan divided into Northern, Central, Southern and unattributed (NW  
845 Kalimantan) from Williams and Harahap (1987) and Harahap (1993). Basalt and basaltic andesite  
846 from Tawau on the Semporna Peninsula, NE Borneo (Macpherson et al., 2010). Hydrated basalt  
847 melting experiments at high-pressure under fluid-present melting conditions (H<sub>2</sub>O-pres; Winther and  
848 Newton, 1991), and dehydration melting conditions at and above 8 kbar (DehydMelt; Rapp and  
849 Watson, 1995). In panel b) only experimental equilibration of slab melt with peridotite (AB-1 + AVX;  
850 Rapp et al., 1999). ASI is aluminium saturation index  $[Al / (Ca + Na + K)]$ .

851 Fig. 6: Incompatible trace elements contents of Borneo igneous rocks normalised to N-MORB (Sun  
852 and McDonough 1989). a) Intrusive rocks from Kuching. b) Volcanic rocks from Kuching with one  
853 Kuching intrusive rock (TB 58) for comparison. c) Bau intrusive rocks with Kuching intrusive (TB 58)

854 for comparison. d) Intermediate rocks from Kuching and Bau compared to representative rocks from  
855 Northern (N), Central (C), and Southern (S) groups of Kalimantan Sintang intrusives (Harahap, 1993).  
856 Comparators from different locations were chosen for their similar SiO<sub>2</sub> to the specimens from the  
857 primary location displayed on each panel.

858 Fig. 7: a) Incompatible trace elements normalised to N-MORB (Sun and McDonough 1989) for the  
859 least silicic sample from Kuching (TB 23) compared with basaltic or basaltic andesite sample from the  
860 Northern and Southern Sintang groups of Kalimantan (Harahap, 1993) and Semporna Peninsula, NE  
861 Borneo (Macpherson et al., 2010). b) Y vs Sr/Y plot showing the adakite field (after Defant and  
862 Drummond, 1990). Shaded areas are literature data from \*Prouteau et al. (2001) and Williams and  
863 Harahap (1987) and \*\*Thompson et al. (1994), Simmons and Browne (1990), Harahap (1993),  
864 Heryanto et al. (1993) and Moss et al. (1998). Bau Suite samples fall predominantly in the adakite  
865 field, while the West Sarawak Sintang Suite samples are mainly outside the field.

866 Fig. 8: U-Pb zircon age dating for the West Sarawak Sintang Suite - intrusive rocks. a) Sample TB63b  
867 dated as  $21.1 \pm 0.2$  Ma. b) Sample TB58 dated as  $20.3 \pm 0.2$  Ma. c) Sample TB33 dated as  $20.1 \pm 0.2$   
868 Ma. Colour code for circles in the Tera-Wasserburg plot: red – concordant, black – discordant, grey –  
869 concordant, discount for weighted mean age calculation due to inheritance, large uncertainty or  
870 slight Pb loss.

871 Fig. 9: U-Pb zircon age dating for the West Sarawak Sintang Suite - volcanic rocks (a, b) and the Bau  
872 Suite (c, d). a) Sample TB141 dated as  $19.8 \pm 0.3$  Ma. A slightly older population is dated as  $21.5 \pm 0.4$   
873 Ma. Only concordant ages are displayed. b) Sample TB209a dated as  $18.6 \pm 0.2$  Ma. c) Sample TB9 is  
874 dated as  $14.1 \pm 0.1$  Ma (only 24 ages are displayed to improve the display). d) Sample TB61 is dated  
875 as  $12.4 \pm 0.9$  Ma. Both samples have a younger zircon at c. 5 Ma that is interpreted as lead-loss due  
876 to hydrothermal overprint.

877 Fig. 10: a) Summary of high precision ages for the Neogene magmatism in Borneo. Red colour  
878 indicates crystallisation ages. Yellow colour indicates inheritance (slightly older ages). For inheritance

879 ages of Phanerozoic to Precambrian age see Figure 13. (Note: Period/Epoch is not to scale). \* Mukah  
880 tuff U-Pb zircon LA-ICP-MS data from Ramkumar et al. (2018). \*\* Kelian volcanics U-Pb LA-ICP-MS  
881 zircon data from Setiabudi et al. (2007) and Davies et al. (2008). \*\*\* Temburong tuff U-Pb zircon LA-  
882 ICP-MS data (S. Burley, pers. comm., 2018). b) Age histogram of all inherited U-Pb zircon ages  
883 analysed in the upper Cenozoic magmatic rocks derived by re-melting of basement. Mesozoic ages  
884 resemble the Schwaner Mountains, the Jagoi Granodiorite, the Sadong and Kuching Formations and  
885 other Triassic rocks of NW Kalimantan (Davies et al., 2014; Breitfeld et al., 2017; Hennig et al., 2017).  
886 Proterozoic ages indicate a heterogeneous basement.

887 Fig. 11: a) Schematic diagram of western Borneo showing the genesis of adakitic and non-adakitic  
888 melts. Mantle upwelling into lithospheric thin spot results in melting of crust and intra-plate basalt at  
889 various depths. The zones of melting are bounded by deep rooted faults that are associated with the  
890 large sedimentary basins in Kalimantan (Melawi) and Kalimantan-Sarawak (Ketungau). b) Schematic  
891 block diagram of the Neogene magmatism in West Sarawak. Early Miocene Sintang Suite associated  
892 with the Lupar fault trend is dominated by non-adakitic melts. Melting occurs above the garnet-in  
893 boundary. Middle Miocene Bau Suite is associated with the Bau fault trend and dominated by  
894 adakitic melts. Melting occurs in deeper levels below the garnet-in boundary.

895

896

### 897 **Table Captions**

898 Tab. 1: Major and trace element concentrations for West Sarawak Sintang Suite and Bau Suite. All  
899 data from XRF analyses, except <sup>a)</sup>, which are from ICP-MS analyses. LOI = loss on ignition.  
900 (\*\*estimated uncertainty is the largest of the absolute  $\pm$  error and the percentage error.)

901 Tab. 2: Summary of U-Pb zircon dating of this study, subdividing the Neogene igneous rocks into the  
902 Lower Miocene West Sarawak Sintang Suite (intrusive and volcanic rocks) and into the Middle  
903 Miocene Bau Suite.

904 **References**

- 905 Andersen, T., 2002. Correction of common lead in U–Pb analyses that do not report <sup>204</sup>Pb.  
906 *Chemical Geology* 192, 59-79.
- 907 Beard, J.S., Lofgren, G.E., 1991. Dehydration melting and water-saturated melting of basaltic and  
908 andesitic greenstones and amphibolites at 1, 3, and 6. 9 kb. *Journal of Petrology* 32, 365-401.
- 909 Bladon, G.M., Pieters, P.E., Supriatna, S., 1989. Catalogue of isotopic ages commissioned by the  
910 Indonesia-Australia Geological Mapping Project for igneous and metamorphic rocks in Kalimantan,  
911 Preliminary Report. Geological Research and Development Centre, Bandung.
- 912 Bouilhol, P., Magni, V., van Hunen, J., Kaislaniemi, L., 2015. A numerical approach to melting in warm  
913 subduction zones. *Earth and Planetary Science Letters* 411, 37-44.
- 914 Breifeld, H.T., Hall, R., 2018. The eastern Sundaland margin in the latest Cretaceous to Late Eocene:  
915 Sediment provenance and depositional setting of the Kuching and Sibuluan Zones of Borneo. *Gondwana  
916 Research* 63, 34-64.
- 917 Breifeld, H.T., Hall, R., Galin, T., BouDagher-Fadel, M.K., 2018. Unravelling the stratigraphy and  
918 sedimentation history of the uppermost Cretaceous to Eocene sediments of the Kuching Zone in  
919 West Sarawak (Malaysia), Borneo. *Journal of Asian Earth Sciences* 160, 200-223.
- 920 Breifeld, H.T., Hall, R., Galin, T., Forster, M.A., BouDagher-Fadel, M.K., 2017. A Triassic to Cretaceous  
921 Sundaland–Pacific subduction margin in West Sarawak, Borneo. *Tectonophysics* 694, 35-56.
- 922 Bryan, S.E., Ernst, R.E., 2008. Revised definition of large igneous provinces (LIPs). *Earth-Science  
923 Reviews* 86, 175-202.
- 924 Calzia, J.P., Rämö, O.T., 2000. Late Cenozoic crustal extension and magmatism, southern Death  
925 Valley region, California. *Great Basin and Sierra Nevada: Geological Society of America Field Guide* 2,  
926 135-164.

927 Campbell, I.H., Taylor, S.R., 1983. No water, no granites-No oceans, no continents. *Geophysical*  
928 *Research Letters* 10, 1061-1064.

929 Castillo, P.R., Janney, P.E., Solidum, R.U., 1999. Petrology and geochemistry of Camiguin Island,  
930 southern Philippines: insights to the source of adakites and other lavas in a complex arc setting.  
931 *Contributions to Mineralogy and Petrology* 134, 33-51.

932 Chung, S.-L., Liu, D., Ji, J., Chu, M.-F., Lee, H.-Y., Wen, D.-J., Lo, C.-H., Lee, T.-Y., Qian, Q., Zhang, Q.,  
933 2003. Adakites from continental collision zones: melting of thickened lower crust beneath southern  
934 Tibet. *Geology* 31, 1021-1024.

935 Coffin, M.F., Eldholm, O., 1994. Large igneous provinces: crustal structure, dimensions, and external  
936 consequences. *Reviews of Geophysics* 32, 1-36.

937 Conrad, C.P., Bianco, T.A., Smith, E.I., Wessel, P., 2011. Patterns of intraplate volcanism controlled by  
938 asthenospheric shear. *Nature Geoscience* 4, 317-321.

939 Conrad, C.P., Wu, B., Smith, E.I., Bianco, T.A., Tibbetts, A., 2010. Shear-driven upwelling induced by  
940 lateral viscosity variations and asthenospheric shear: A mechanism for intraplate volcanism. *Physics*  
941 *of the Earth and Planetary Interiors* 178, 162-175.

942 Cullen, A., Macpherson, C., Taib, N.I., Burton-Johnson, A., Geist, D., Spell, T., Banda, R.M., 2013. Age  
943 and petrology of the Usun Apau and Linau Balui volcanics: Windows to central Borneo's interior.  
944 *Journal of Asian Earth Sciences* 76, 372-388.

945 Davies, A.G.S., 2002. *Geology and genesis of the Kellan gold Deposit, East Kalimantan, Indonesia.*  
946 University of Tasmania, Tasmania, Australia, p. 404.

947 Davies, A.G.S., Cooke, D.R., Gemmell, J.B., van Leeuwen, T., Cesare, P., Hartshorn, G., 2008.  
948 Hydrothermal breccias and veins at the Kelian gold mine, Kalimantan, Indonesia: genesis of a large  
949 epithermal gold deposit. *Economic Geology* 103, 717-757.

950 Davies, L., Hall, R., Armstrong, R., 2014. Cretaceous crust in SW Borneo: petrological, geochemical  
951 and geochronological constraints from the Schwaner Mountains, Proceedings Indonesian Petroleum  
952 Association, 38th Annual Convention and Exhibition, IPA14-G-025.

953 Defant, M.J., Drummond, M.S., 1990. Derivation of some modern arc magmas by melting of young  
954 subducted lithosphere. *Nature* 347, 662-665.

955 Douth, H.F., 1992. Aspects of the structural histories of the Tertiary sedimentary basins of East,  
956 Central and West Kalimantan and their margins. *BMR Journal of Australian Geology and Geophysics*  
957 13, 237-250.

958 Drummond, M.S., Defant, M.J., Kepezhinskas, P.K., 1996. Petrogenesis of slab-derived trondhjemite–  
959 tonalite–dacite/adakite magmas. *Earth and Environmental Science Transactions of the Royal Society*  
960 *of Edinburgh* 87, 205-215.

961 Ekici, T., Macpherson, C.G., Otlu, N., 2012. Polybaric melting of a single mantle source during the  
962 Neogene Siverek phase of the Karacadağ Volcanic Complex, SE Turkey. *Lithos* 146, 152-163.

963 Ekici, T., Macpherson, C.G., Otlu, N., Fontignie, D., 2014. Foreland Magmatism during the Arabia–  
964 Eurasia Collision: Pliocene–Quaternary Activity of the Karacadağ Volcanic Complex, SW Turkey.  
965 *Journal of Petrology* 55, 1753-1777.

966 Frost, B.R., Barnes, C.G., Collins, W.J., Arculus, R.J., Ellis, D.J., Frost, C.D., 2001. A Geochemical  
967 Classification for Granitic Rocks. *Journal of Petrology* 42, 2033-2048.

968 Galin, T., Breitfeld, H.T., Hall, R., Sevastjanova, I., 2017. Provenance of the Cretaceous–Eocene  
969 Rajang Group submarine fan, Sarawak, Malaysia from light and heavy mineral assemblages and U-Pb  
970 zircon geochronology. *Gondwana Research* 51, 209-233.

971 Griffin, W.L., Powell, W.J., Pearson, N.J., O'Reilly, S.Y., 2008. GLITTER: data reduction software for  
972 laser ablation ICP-MS, in: Sylvester, P.J. (Ed.), *Laser Ablation-ICP-MS in the earth sciences: current*

973 practices and outstanding issues Mineralogical association of Canada, short course series 40, pp.  
974 308-311.

975 Guo, Z., Wilson, M., Liu, J., 2007. Post-collisional adakites in south Tibet: products of partial melting  
976 of subduction-modified lower crust. *Lithos* 96, 205-224.

977 Hageman, H., 1987. Palaeobathymetrical changes in NW Sarawak during Oligocene to Pliocene.  
978 *Geological Society of Malaysia Bulletin* 21, 91-102.

979 Haile, N.S., 1974. Borneo, in: Spencer, A.M. (Ed.), *Mesozoic-Cenozoic Orogenic Belts*, pp. 333-347.

980 Haile, N.S., Lam, S.K., Banda, R.M., 1994. Relationship of gabbro and pillow lavas in the Lupar  
981 Formation, West Sarawak: Implications for interpretation of the Lubok Antu Melange and the Lupar  
982 Line. *Bulletin of the Geological Society of Malaysia* 36, 1-9.

983 Haile, N.S., McElhinny, M.W., McDougall, I., 1977. Palaeomagnetic data and radiometric ages from  
984 the Cretaceous of West Kalimantan (Borneo), and their significance in interpreting regional  
985 structure. *Journal of the Geological Society of London* 133, 133-144.

986 Hall, R., 2012. Late Jurassic–Cenozoic reconstructions of the Indonesian region and the Indian Ocean.  
987 *Tectonophysics* 570–571, 1-41.

988 Hall, R., 2013. Contraction and extension in northern Borneo driven by subduction rollback. *Journal*  
989 *of Asian Earth Sciences* 76, 399-411.

990 Hall, R., Breitfeld, H.T., 2017. The Demise of the Proto-South China Sea. *Geological Society of*  
991 *Malaysia Bulletin* 63, 61-76.

992 Hall, R., Sevastjanova, I., 2012. Australian crust in Indonesia. *Australian Journal of Earth Sciences* 59,  
993 827-844.

994 Hall, R., Spakman, W., 2015. Mantle structure and tectonic history of SE Asia. *Tectonophysics* 658,  
995 14-45.

996 Hall, R., van Hattum, M.W.A., Spakman, W., 2008. Impact of India–Asia collision on SE Asia: the  
997 record in Borneo. *Tectonophysics* 451, 366-389.

998 Hamilton, W., 1979. *Tectonics of the Indonesian region*. U.S.G.S. Prof. Paper 1078, 345pp.

999 Harahap, B.H., 1993. Geochemical investigation of Tertiary, magmatism rocks from Central West  
1000 Kalimantan, Indonesia, 22nd Annual Convention, Indonesian Association of Geologists, pp. 304-326.

1001 Harahap, B.H., 1994. Petrology and Geochemistry of Mount Niut Volcano West Kalimantan.  
1002 Geological Research and Development Center, Indonesian Department of Mines and Energy 17, 1-  
1003 12.

1004 Hartono, U., 2006. Petrogenesis of the Sintang Intrusives and its implications for mineralization in  
1005 Northwest Kalimantan. *Jurnal Geologi dan Sumberdaya Mineral* 16, 210-219.

1006 Haschke, M., Ben-Avraham, Z., 2005. Adakites from collision-modified lithosphere. *Geophysical*  
1007 *Research Letters* 32, L15302.

1008 Hassan, M.H.A., Johnson, H.D., Allison, P.A., Abdullah, W.H., 2013. Sedimentology and stratigraphic  
1009 development of the upper Nyalau Formation (Early Miocene), Sarawak, Malaysia: a mixed wave-and  
1010 tide-influenced coastal system. *Journal of Asian Earth Sciences* 76, 301-311.

1011 Heng, Y.E., 1992. *Geological Map of Sarawak, 1:500,000*. Geological Survey of Malaysia.

1012 Hennig, J., Breitfeld, H.T., Hall, R., Nugraha, A.M.S., 2017. The Mesozoic tectono-magmatic evolution  
1013 at the Paleo-Pacific subduction zone in West Borneo. *Gondwana Research* 48, 292-310.

1014 Hennig-Breitfeld, J., Breitfeld, H.T., Hall, R., BouDagher-Fadel, M.K., Thirlwall, M., 2019. A new upper  
1015 Paleogene to Neogene stratigraphy for NW Borneo: Paleogeography of the eastern Sundaland  
1016 margin. *Earth-Science Reviews* 190, 1-32.

1017 Heryanto, R., Williams, P.R., Harahap, B.H., Pieters, P.E., 1993. *Geology of the Sintang sheet area,*  
1018 *Kalimantan, explanatory note and geological map*. Geological Research and Development Center,  
1019 Indonesian Department of Mines and Energy.

1020 Hou, Z.Q., Gao, Y.F., Qu, X.M., Rui, Z.Y., Mo, X.X., 2004. Origin of adakitic intrusives generated during  
1021 mid-Miocene east–west extension in southern Tibet. *Earth and Planetary Science Letters* 220, 139-  
1022 155.

1023 Hussein, M., Serpa, L., Doser, D., Velasco, A., 2011. Imaging the Deep Structure of the Central Death  
1024 Valley Basin Using Receiver Function, Gravity, and Magnetic Data. *International Journal of*  
1025 *Geosciences* 2, 676.

1026 Hutchison, C.S., 1996. The 'Rajang Accretionary Prism' and 'Lupar Line' Problem of Borneo, in: Hall,  
1027 R., Blundell, D.J. (Eds.), *Tectonic Evolution of SE Asia*, pp. 247-261.

1028 Hutchison, C.S., 2005. *Geology of North-West Borneo. Sarawak, Brunei and Sabah.*, First Edition ed.  
1029 Elsevier, Amsterdam, Netherlands.

1030 Hutchison, C.S., 2010. Oroclines and paleomagnetism in Borneo and south-east Asia. *Tectonophysics*  
1031 496, 53-67.

1032 JICA, 1985. Report on the collaborative mineral exploration of the Bau area, west Sarawak, Published  
1033 report. Metal Mining Agency of Japan, Tokyo, p. 97 pp.

1034 Johnson, R.W., Mackenzie, D.E., Smith, I.E.M., 1978. Delayed partial melting of subduction-modified  
1035 mantle in Papua New Guinea. *Tectonophysics* 46, 197-216.

1036 Kay, R.W., 1978. Aleutian magnesian andesites: melts from subducted Pacific Ocean crust. *Journal of*  
1037 *Volcanology and Geothermal Research* 4, 117-132.

1038 Kelemen, P.B., 1995. Genesis of high Mg# andesites and the continental crust. *Contributions to*  
1039 *Mineralogy and Petrology* 120, 1-19.

1040 King, S.D., Anderson, D.L., 1998. Edge-driven convection. *Earth and Planetary Science Letters* 160,  
1041 289-296.

1042 Kirk, H.J.C., 1968. The igneous rocks of Sarawak and Sabah. Geological Survey of Malaysia, Borneo  
1043 Region, Bulletin 5, 210 pp.

- 1044 Kirwin, D.J., Royle, D.Z., 2019. Sediment-Hosted Gold Deposits in Southeast Asia. *Resource Geology*  
1045 69, 125-147.
- 1046 Liechti, P., Roe, F.W., Haile, N.S., 1960. The Geology of Sarawak, Brunei and the western part of  
1047 North Borneo. British Territories of Borneo, Geological Survey Department, Bulletin (Two volumes)  
1048 3, 360 pp.
- 1049 Ludwig, K.R., 2003. User's Manual for Isoplot 3.00. A Geochronological Toolkit for Microsoft Excel,  
1050 Berkeley Geochronology Center, Berkeley, CA.
- 1051 Macpherson, C.G., 2008. Lithosphere erosion and crustal growth in subduction zones: Insights from  
1052 initiation of the nascent East Philippine Arc. *Geology* 36, 311-314.
- 1053 Macpherson, C.G., Chiang, K.K., Hall, R., Nowell, G.M., Castillo, P.R., Thirlwall, M.F., 2010. Plio-  
1054 Pleistocene intra-plate magmatism from the southern Sulu Arc, Semporna peninsula, Sabah, Borneo:  
1055 Implications for high-Nb basalt in subduction zones. *Journal of Volcanology and Geothermal*  
1056 *Research* 190, 25-38.
- 1057 Macpherson, C.G., Dreher, S.T., Thirlwall, M.F., 2006. Adakites without slab melting: high pressure  
1058 differentiation of island arc magma, Mindanao, the Philippines. *Earth and Planetary Science Letters*  
1059 243, 581-593.
- 1060 Madon, M.B.H., 1999. Basin types, tectono-stratigraphic provinces and structural styles. *The*  
1061 *Petroleum Geology and Resources of Malaysia*, 77-112.
- 1062 Martin, H., 1999. Adakitic magmas: modern analogues of Archaean granitoids. *Lithos* 46, 411-429.
- 1063 Martin, H., Smithies, R.H., Rapp, R., Moyen, J.F., Champion, D., 2005. An overview of adakite,  
1064 tonalite–trondhjemite–granodiorite (TTG), and sanukitoid: relationships and some implications for  
1065 crustal evolution. *Lithos* 79, 1-24.
- 1066 McKenzie, D., Bickle, M.J., 1988. The volume and composition of melt generated by extension of the  
1067 lithosphere. *Journal of Petrology* 29, 625-679.

1068 Monaghan, A.A., Parrish, R.R., 2006. Geochronology of Carboniferous–Permian magmatism in the  
1069 Midland Valley of Scotland: implications for regional tectonomagmatic evolution and the numerical  
1070 time scale. *Journal of the Geological Society* 163, 15-28.

1071 Moss, S.J., Carter, A., Baker, S., Hurford, A.J., 1998. A Late Oligocene tectono-volcanic event in East  
1072 Kalimantan and the implications for tectonics and sedimentation in Borneo. *Journal of the Geological*  
1073 *Society* 155, 177-192.

1074 Nemchin, A.A., Cawood, P.A., 2005. Discordance of the U–Pb system in detrital zircons: implication  
1075 for provenance studies of sedimentary rocks. *Sedimentary Geology* 182, 143-162.

1076 Ottley, C.J., Pearson, D.G., Irvine, G.J., 2003. A routine method for the dissolution of geological  
1077 samples for the analysis of REE and trace elements via ICP-MS. In: Holland, J.C., Tanner, S.D. (Eds)  
1078 *Plasma Source Mass Spectrometry: Applications and Emerging Technologies*. Cambridge: Royal  
1079 *Society of Chemistry*, 221-230.

1080 Pearce, N.J.G., Perkins, W.T., Westgate, J.A., Gorton, M.P., Jackson, S.E., Neal, C.R., Chenery, S.P.,  
1081 1997. A Compilation of New and Published Major and Trace Element Data for NIST SRM 610 and  
1082 NIST SRM 612 Glass Reference Materials. *Geostandards Newsletter* 21, 115-144.

1083 Pieters, P.E., Sanyoto, P., 1993. Geology of the Pontianak/Nangataman Sheet area, Kalimantan. Map  
1084 at 1:250000 scale. Geological Research and Development Centre, Bandung.

1085 Pieters, P.E., Trail, D.S., Supriatna, S., 1987. Correlation of Early Tertiary rocks across Kalimantan.  
1086 Indonesian Petroleum Association, Proceedings 16th annual convention Jakarta, 1987 I, 291-306.

1087 Plank, T., Cooper, L.B., Manning, C.E., 2009. Emerging geothermometers for estimating slab surface  
1088 temperatures. *Nature Geoscience* 2, 611.

1089 Prouteau, G., Maury, R.C., Rangin, C., Suparka, E., Bellon, H., Pubellier, M., Cotten, J., 1996. Les  
1090 adakites miocènes du NW de Bornéo, témoins de la fermeture de la proto-mer de Chine. *Comptes*  
1091 *rendus de l'Académie des sciences. Série 2. Sciences de la terre et des planètes* 323, 925-932.

1092 Prouteau, G., Maury, R.C., Sajona, F.G., Pubellier, M., Cotten, J., Bellon, H., 2001. Le magmatisme  
1093 post-collisionnel du Nord-Ouest de Bornéo, produit de la fusion d'un fragment de croûte océanique  
1094 ancré dans le manteau supérieur. *Bulletin de la Société Géologique de France* 172, 319-332.

1095 Ramkumar, M., Santosh, M., Nagarajan, R., Li, S.S., Mathew, M., Menier, D., Siddiqui, N., Rai, J.,  
1096 Sharma, A., Farroqui, S., 2018. Late Middle Miocene volcanism in Northwest Borneo, Southeast Asia:  
1097 Implications for tectonics, paleoclimate and stratigraphic marker. *Palaeogeography,*  
1098 *Palaeoclimatology, Palaeoecology* 490, 141-162.

1099 Rangin, C., Spakman, W., Pubellier, M., Bijwaard, H., 1999. Tomographic and geological constraints  
1100 on subduction along the eastern Sundaland continental margin (South-East Asia). *Bulletin de la*  
1101 *Société Géologique de France* 170, 775-788.

1102 Rapp, R.P., Shimizu, N., Norman, M.D., Applegate, G.S., 1999. Reaction between slab-derived melts  
1103 and peridotite in the mantle wedge: experimental constraints at 3.8 GPa. *Chemical Geology* 160,  
1104 335-356.

1105 Rapp, R.P., Watson, E.B., 1995. Dehydration melting of metabasalt at 8–32 kbar: implications for  
1106 continental growth and crust-mantle recycling. *Journal of Petrology* 36, 891-931.

1107 Roberts, G.G., White, N., Hoggard, M.J., Ball, P.W., Meenan, C., 2018. A Neogene history of mantle  
1108 convective support beneath Borneo. *Earth and Planetary Science Letters* 496, 142-158.

1109 Rogers, N.W., Hawkesworth, C.J., Parker, R.J., Marsh, J.S., 1985. The geochemistry of potassic lavas  
1110 from Vulcini, central Italy and implications for mantle enrichment processes beneath the Roman  
1111 region. *Contributions to Mineralogy and Petrology* 90, 244-257.

1112 Sajona, F.G., Maury, R.C., Bellon, H., Cotten, J., Defant, M.J., Pubellier, M., 1993. Initiation of  
1113 subduction and the generation of slab melts in western and eastern Mindanao, Philippines. *Geology*  
1114 21, 1007-1010.

- 1115 Sajona, F.G., Maury, R.C., Pubellier, M., Leterrier, J., Bellon, H., Cotten, J., 2000. Magmatic source  
1116 enrichment by slab-derived melts in a young post-collision setting, central Mindanao (Philippines).  
1117 *Lithos* 54, 173-206.
- 1118 Schmidtke, E.A., Fuller, M., Haston, R.B., 1990. Paleomagnetic data from Sarawak, Malaysian Borneo  
1119 and the Late Mesozoic and Cenozoic tectonics of Sundaland. *Tectonics* 9, 123-140.
- 1120 Schuh, W.D., 1993. *Geology, geochemistry, and ore deposits of the Bau gold mining district,*  
1121 *Sarawak, Malaysia. The University of Arizona, Tucson, USA, 395 pp.*
- 1122 Sen, C., Dunn, T., 1994. Dehydration melting of a basaltic composition amphibolite at 1.5 and 2.0  
1123 GPa: implications for the origin of adakites. *Contributions to Mineralogy and Petrology* 117, 394-409.
- 1124 Setiabudi, B.T., Campbell, I.H., Martin, C.E., Allen, C.M., 2007. Platinum group element geochemistry  
1125 of andesite intrusions of the Kelian region, East Kalimantan, Indonesia: implications of gold depletion  
1126 in the intrusions associated with the Kelian gold deposit. *Economic Geology* 102, 95-108.
- 1127 Setiabudi, B.T., Campbell, I.H., Palin, M.J., 2001. Age of calc-alkaline magmatism associated with the  
1128 Kelian gold deposit. Indonesia: An example of zircon U-Pb dating by excimer laser ablation ICP-MS. A  
1129 *Hydrothermal Odyssey, New Developments in Metalliferous Hydrothermal Systems Research*  
1130 *Conference, 17-19.*
- 1131 Setiawan, B., Le Bel, L.M., 1986. Discovery of a new tin province, Long Laai area, east Kalimantan,  
1132 Indonesia, Exploration and evaluation techniques for Tin/Tungsten granites in Southeast Asia and  
1133 the western Pacific region. *Proceedings of IGCP Project 220 Meeting, pp. 61-82.*
- 1134 Simmons, S.F., Browne, P.R.L., 1990. Mineralogic, alteration and fluid-inclusion studies of epithermal  
1135 gold-bearing veins at the Mt. Muro Prospect, Central Kalimantan (Borneo), Indonesia. *Journal of*  
1136 *Geochemical Exploration* 35, 63-103.
- 1137 Sláma, J., Košler, J., Condon, D.J., Crowley, J.L., Gerdes, A., Hanchar, J.M., Horstwood, M.S.A., Morris,  
1138 G.A., Nasdala, L., Norberg, N., Schaltegger, U., Schoene, B., Tubrett, M.N., Whitehouse, M.J., 2008.

- 1139 Plešovice zircon — A new natural reference material for U–Pb and Hf isotopic microanalysis.  
1140 *Chemical Geology* 249, 1-35.
- 1141 Smith, I.E.M., Taylor, S.R., Johnson, R.W., 1979. REE-fractionated trachytes and dacites from Papua  
1142 New Guinea and their relationship to andesite petrogenesis. *Contributions to Mineralogy and  
1143 Petrology* 69, 227-233.
- 1144 Soeria-Atmadja, R., Noeradi, D., Priadi, B., 1999. Cenozoic magmatism in Kalimantan and its related  
1145 geodynamic evolution. *Journal of Asian Earth Sciences* 17, 25-45.
- 1146 Stern, R.J., 2005. Evidence from ophiolites, blueschists, and ultrahigh-pressure metamorphic  
1147 terranes that the modern episode of subduction tectonics began in Neoproterozoic time. *Geology*  
1148 33, 557-560.
- 1149 Sun, S.S., McDonough, W.-S., 1989. Chemical and isotopic systematics of oceanic basalts:  
1150 implications for mantle composition and processes. Geological Society, London, Special Publications,  
1151 42(1): 313-345.
- 1152 Tan, D.N.K., 1979. Lupar Valley, west Sarawak. Geological Survey of Malaysia, Report 13, 159 pp.
- 1153 Taylor, B., Hayes, D.E., 1983. Origin and history of the South China Sea Basin, in: Hayes, D.E. (Ed.),  
1154 *The Tectonic and Geologic Evolution of Southeast Asian Seas and Islands, Part 2 American  
1155 Geophysical Union*, pp. 23-56.
- 1156 Tera, F., Wasserburg, G.J., 1972. U-Th-Pb systematics in three Apollo 14 basalts and the problem of  
1157 initial Pb in lunar rocks. *Earth and Planetary Science Letters* 14, 281-304.
- 1158 Thompson, R.N., Morrison, M.A., Dickin, A.P., Hendry, G.L., 1983. Continental flood basalts...  
1159 arachnids rule OK? In: Hawkesworth, C.J., Norry, M.J. (Eds.), *Continental basalts and mantle  
1160 xenoliths*. Shiva Geology Series, Nantwich, pp. 158-185.

1161 Thompson, J.F.H., Abidin, H.Z., Both, R.A., Martosuroyo, S., Rafferty, W.J., Thompson, A.J.B., 1994.  
1162 Alteration and epithermal mineralization in the Masupa Ria volcanic center, Central Kalimantan,  
1163 Indonesia. *Journal of Geochemical Exploration* 50, 429-456.

1164 van de Weerd, A., Armin, R.A., Mahadi, S., Ware, P.L.B., 1987. Geologic setting of the Kerendan gas  
1165 and condensate discovery, Tertiary sedimentation and paleogeography of the northwestern part of  
1166 the Kutei Basin, Kalimantan, Indonesia, *Proceedings 16th Annual Convention, Indonesian Petroleum*  
1167 *Association*, pp. 317-338.

1168 van Hattum, M.W.A., Hall, R., Pickard, A.L., Nichols, G.J., 2013. Provenance and geochronology of  
1169 Cenozoic sandstones of northern Borneo. *Journal of Asian Earth Sciences* 76, 266-282.

1170 Van Hunen, J., Moyen, J.-F., 2012. Archean subduction: fact or fiction? *Annual Review of Earth and*  
1171 *Planetary Sciences* 40, 195-219.

1172 van Leeuwen, T.M., Leach, T., Hawke, A.A., Hawke, M.M., 1990. The Kelian disseminated gold  
1173 deposit, east Kalimantan, Indonesia. *Journal of Geochemical Exploration* 35, 1-61.

1174 Williams, P.R., Harahap, B.H., 1987. Preliminary geochemical and age data from post-subduction  
1175 intrusive rocks, northwest Borneo. *Australian Journal of Earth Sciences* 34, 405-416.

1176 Williams, P.R., Johnston, C.R, Almond, R.A., Simamora, W.H., 1988. Late Cretaceous to Early Tertiary  
1177 structural elements of West Kalimantan. *Tectonophysics* 148, 279-298.

1178 Winther, K.T., Newton, R.C., 1991. Experimental melting of hydrous low-K tholeiite: evidence on the  
1179 origin of Archean cratons. *Bull Geol Soc Den* 39, 213-228.

1180 Yogodzinski, G.M., Lees, J.M., Churikova, T.G., Dorendorf, F., Wöerner, G., Volynets, O.N., 2001.  
1181 Geochemical evidence for the melting of subducting oceanic lithosphere at plate edges. *Nature* 409,  
1182 500-504.

1183 Zaw, K.L., Setijadji, L.D., Wardana, I.W., Watanabe, K., 2011. Petrogenetic interpretation of granitoid  
1184 rocks using multicationic parameters in the Sanggau area, Kalimantan island, Indonesia. Journal of  
1185 South East Asian Applied Geology 3, 45-53.

1186

1187

Figure 1



Figure 2

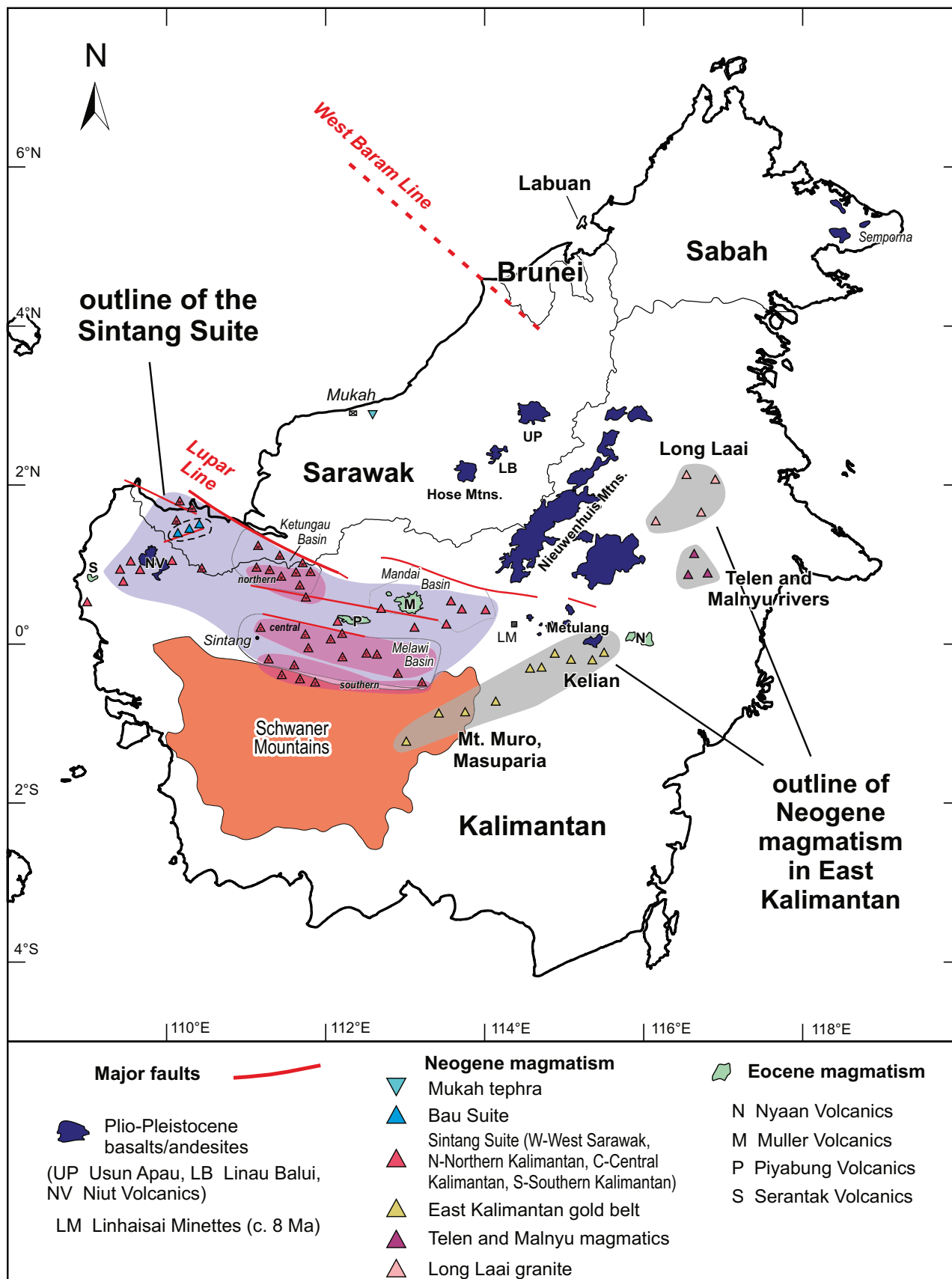


Fig. 2

Figure 3

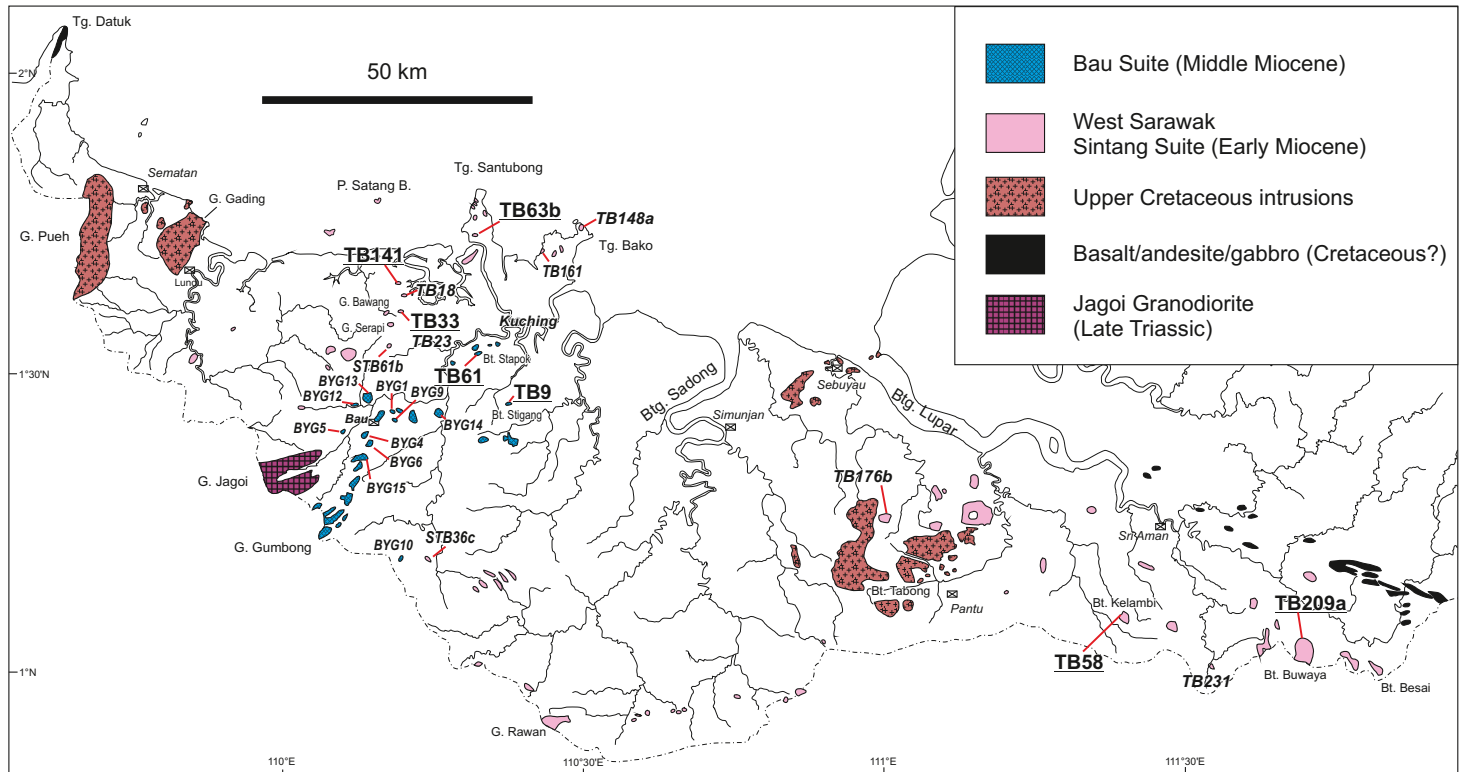


Fig. 3

Figure 4

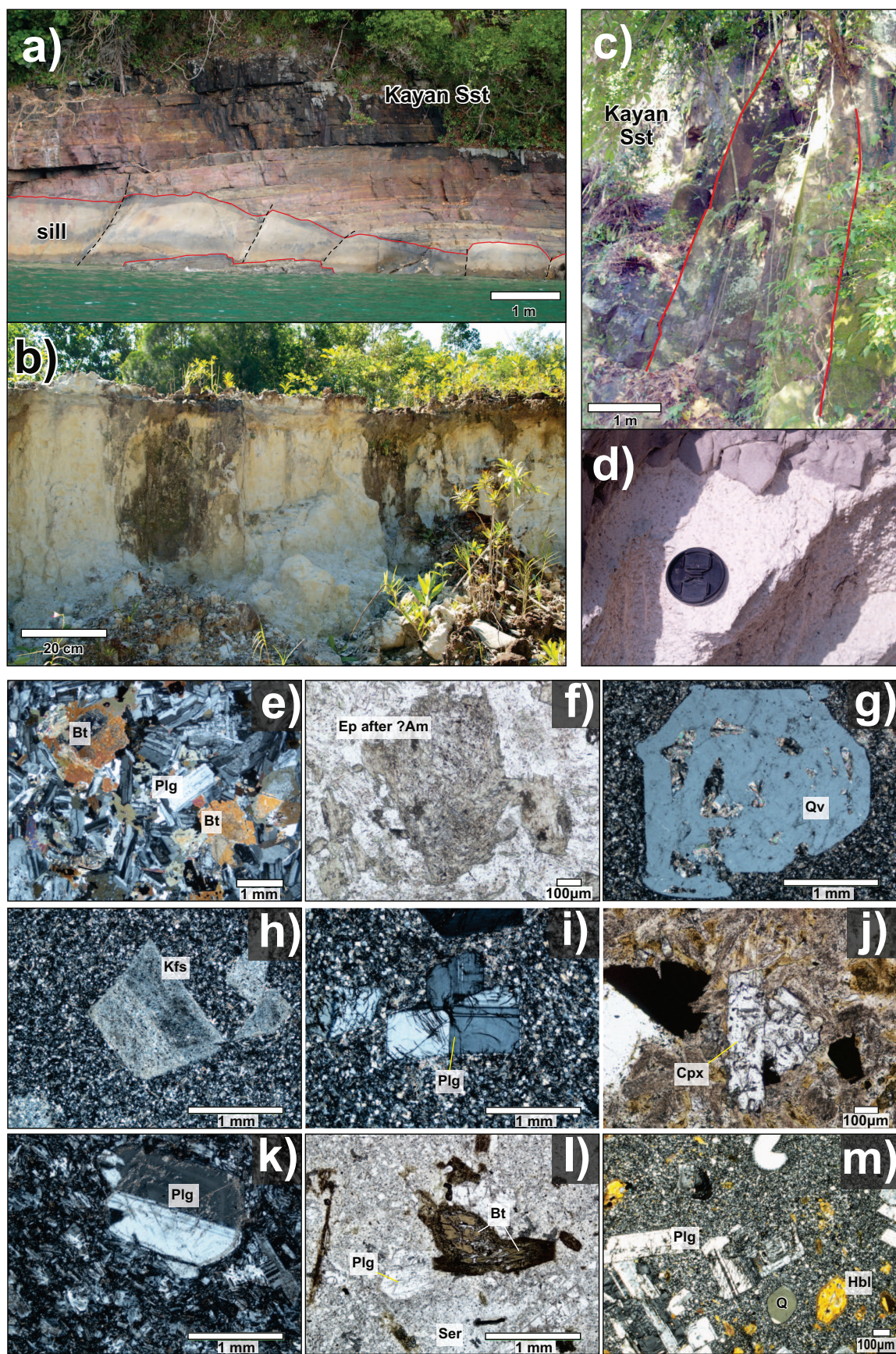
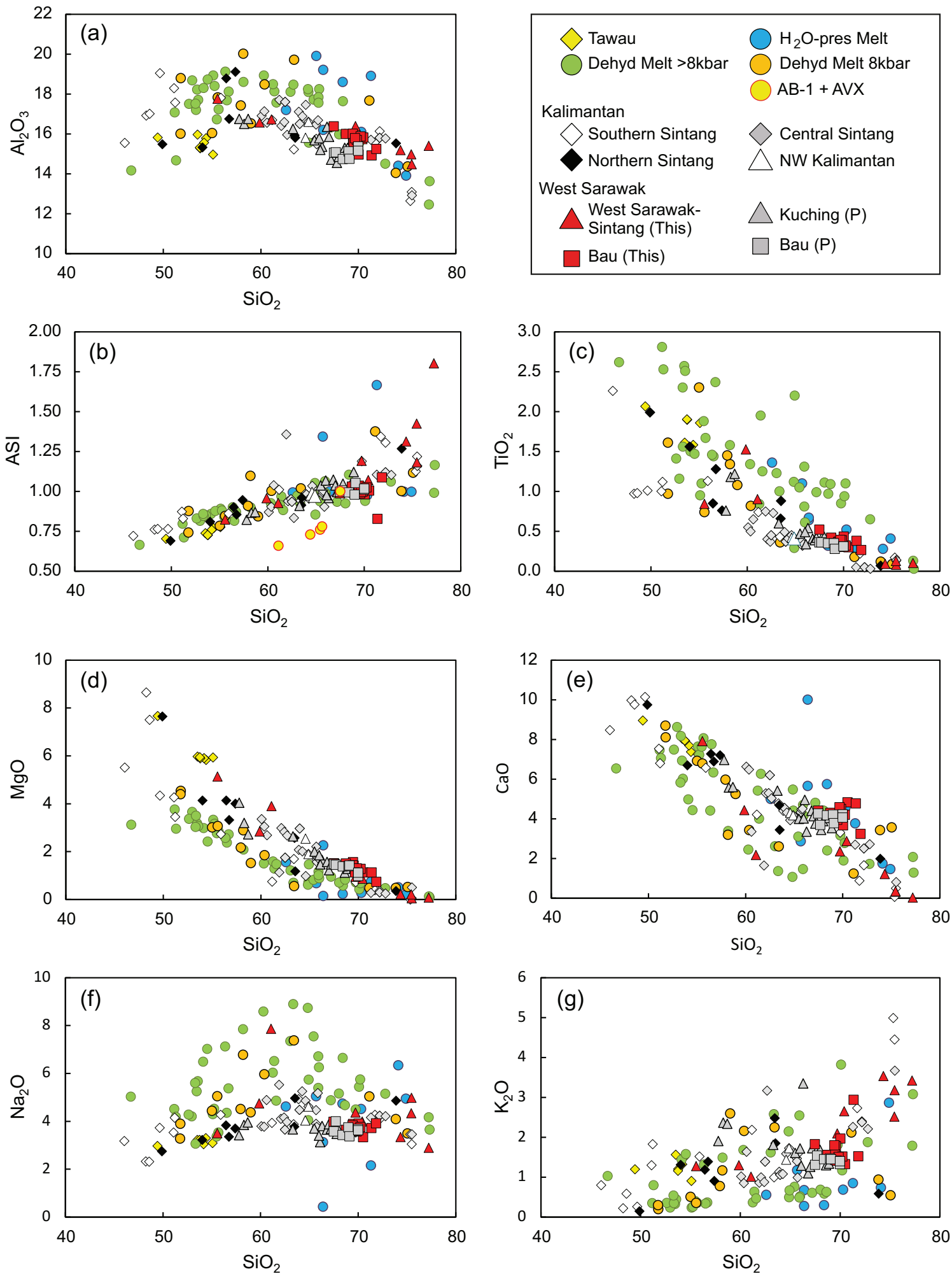


Fig. 4

**Figure 5**

**Figure 6**

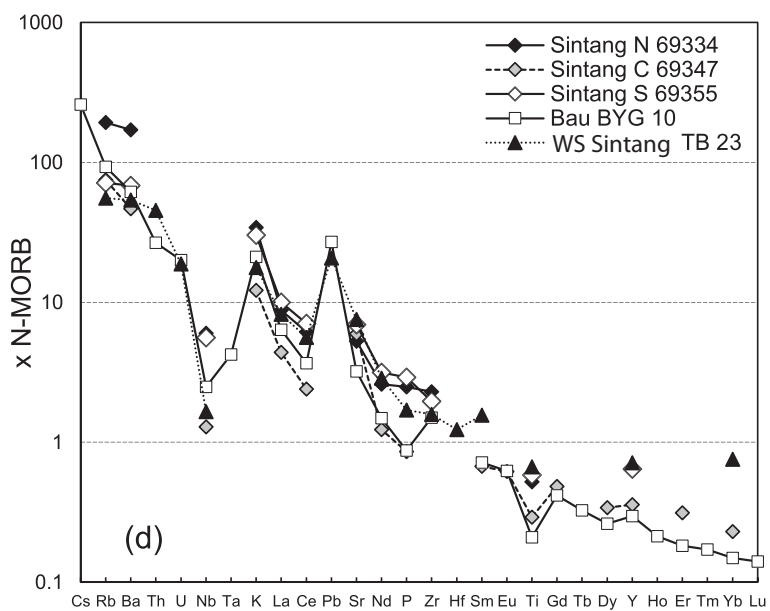
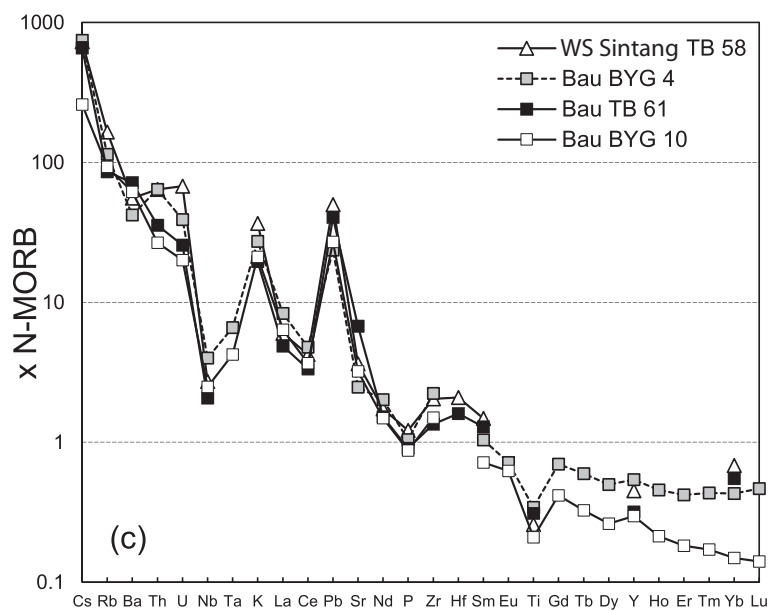
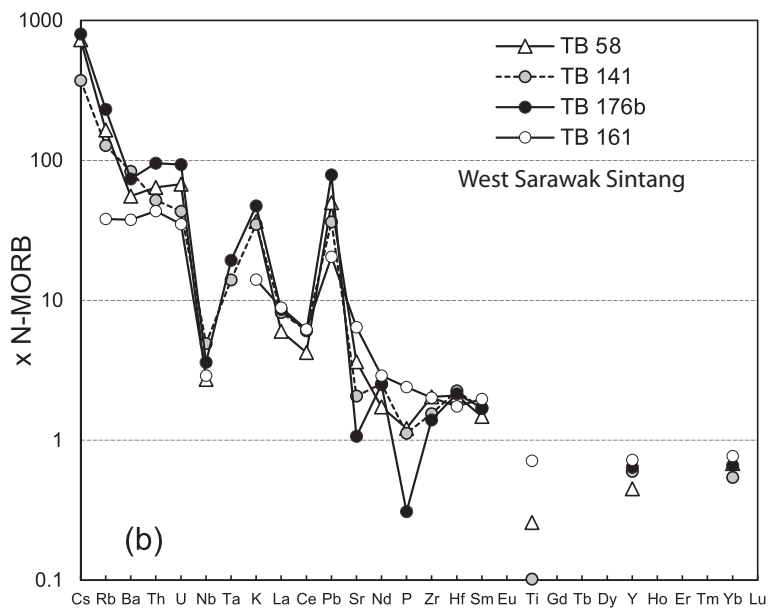
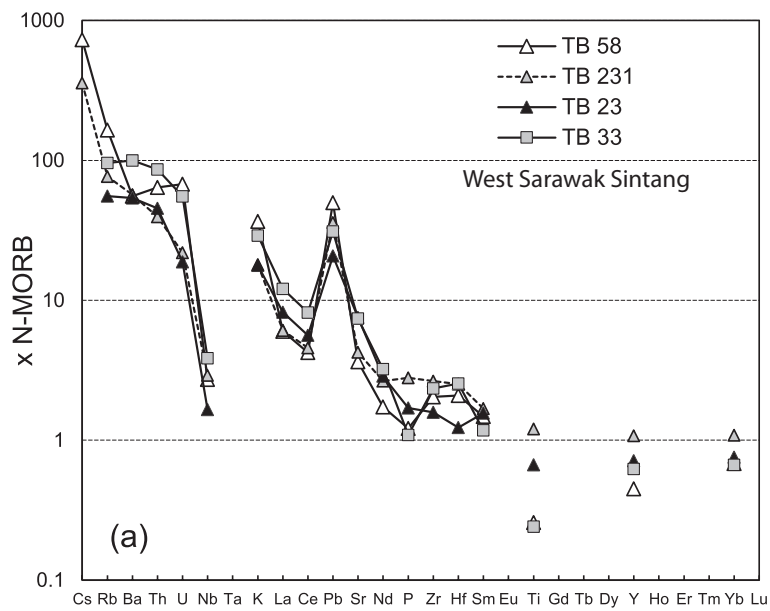


Figure 7

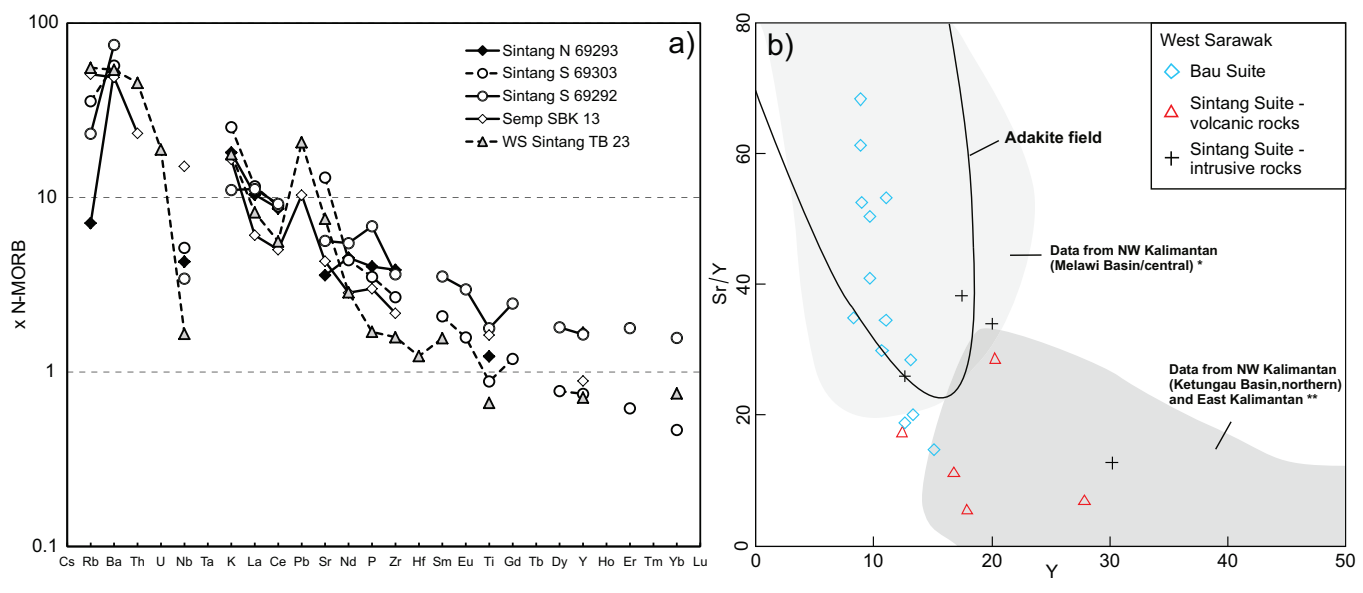


Fig. 7

Figure 8

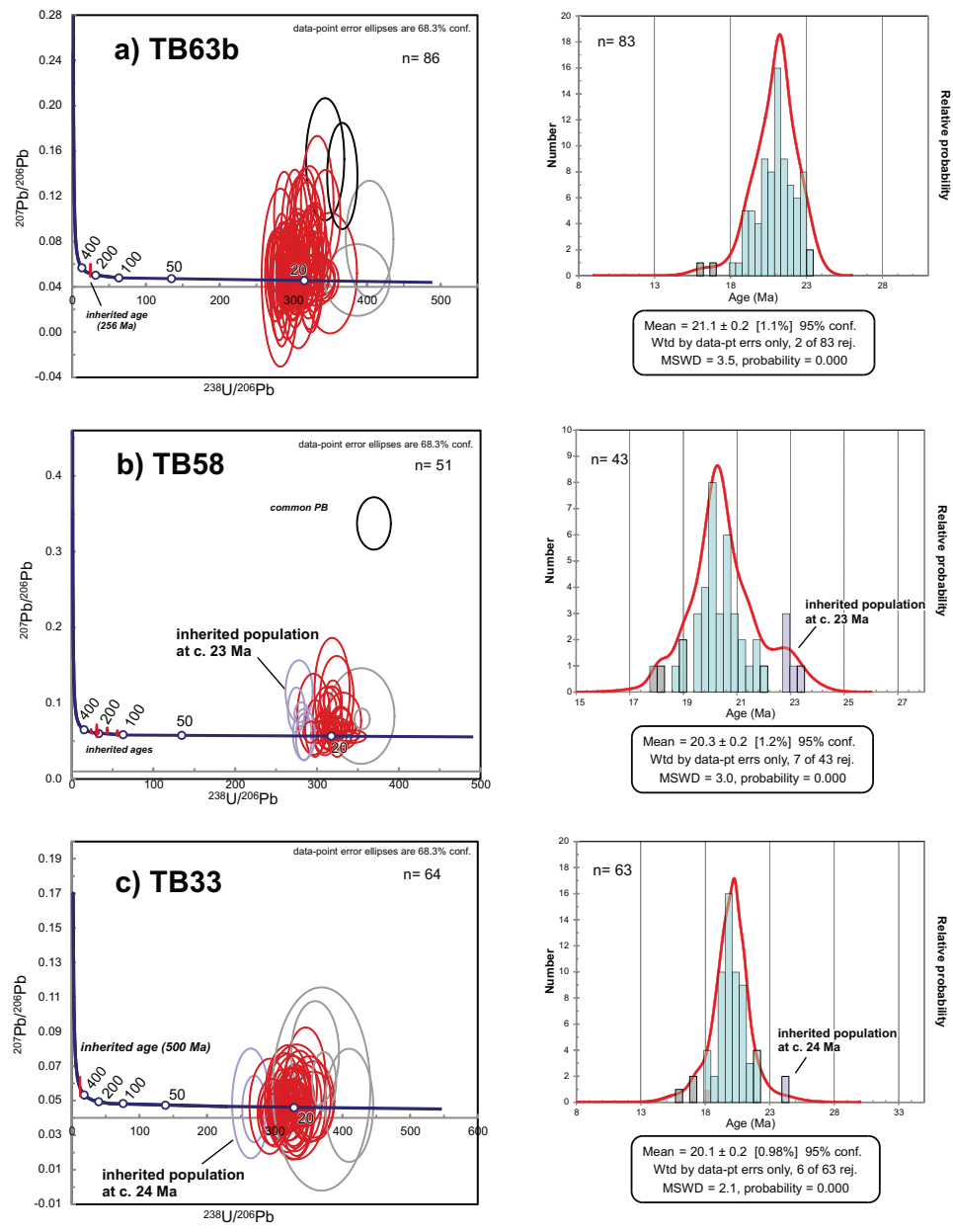


Fig. 8

Figure 9

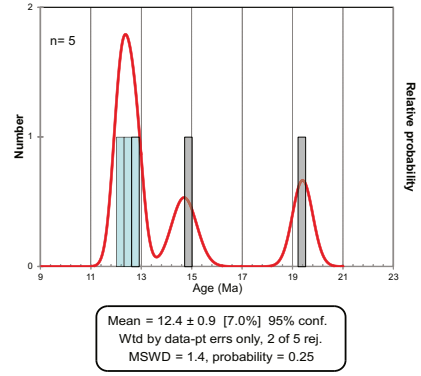
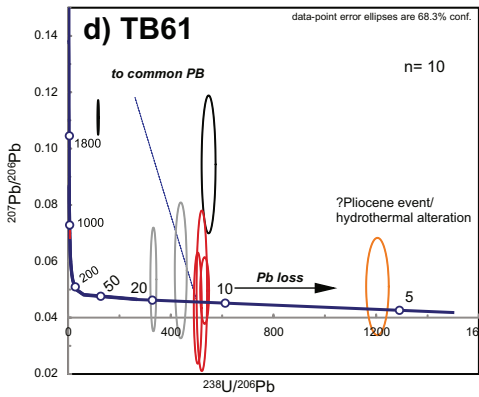
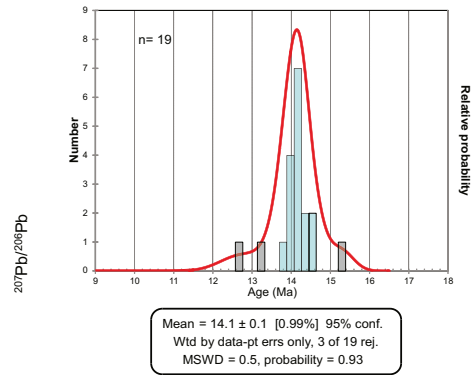
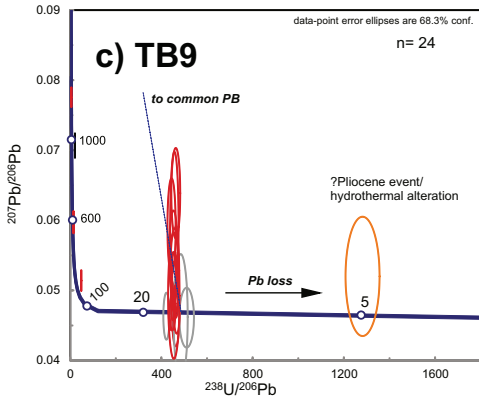
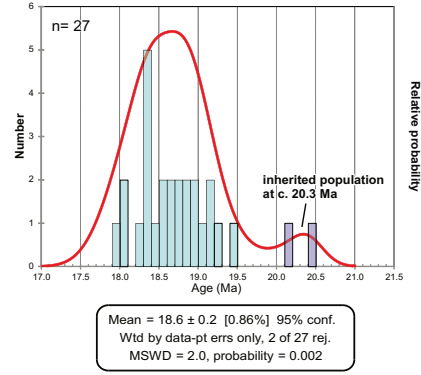
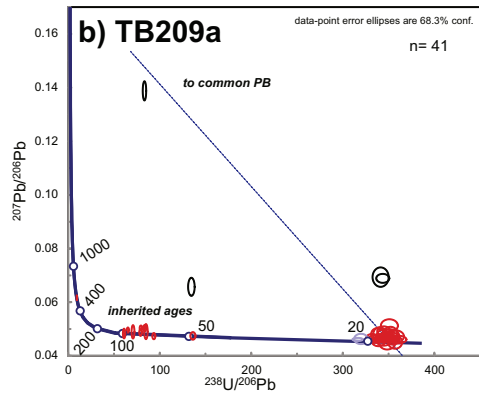
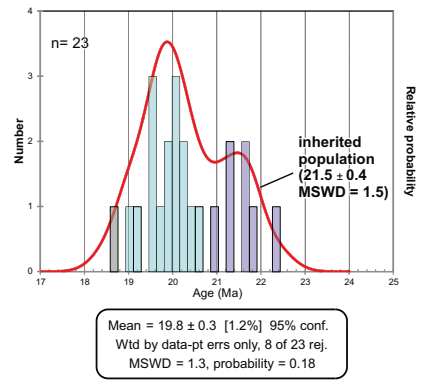
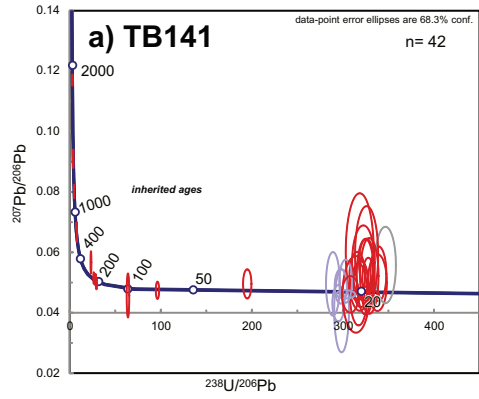


Fig. 9

Figure 10

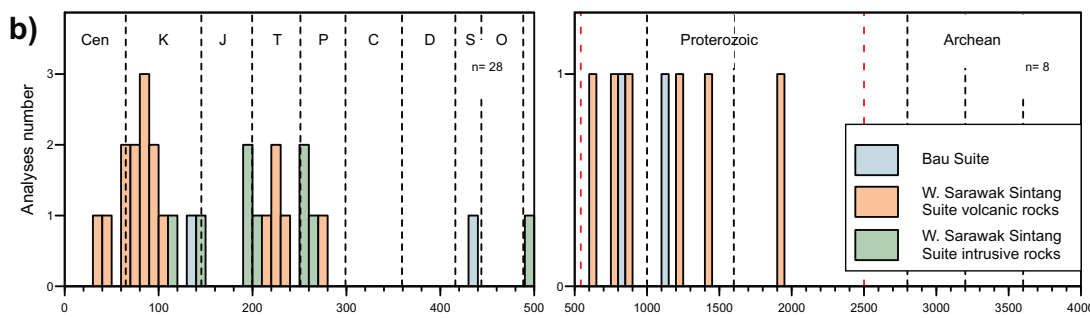
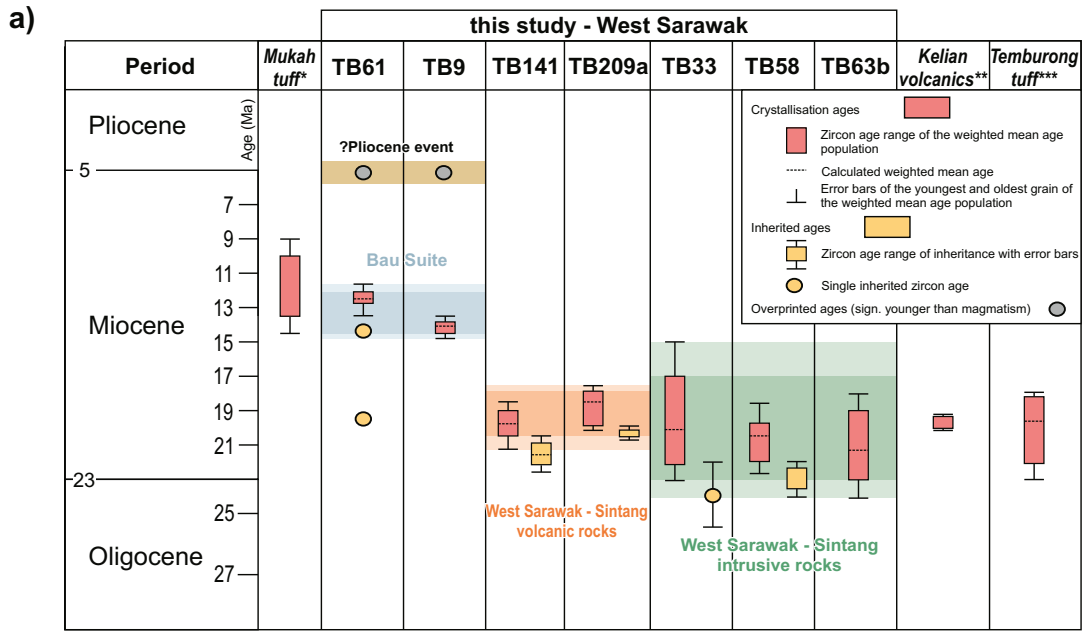
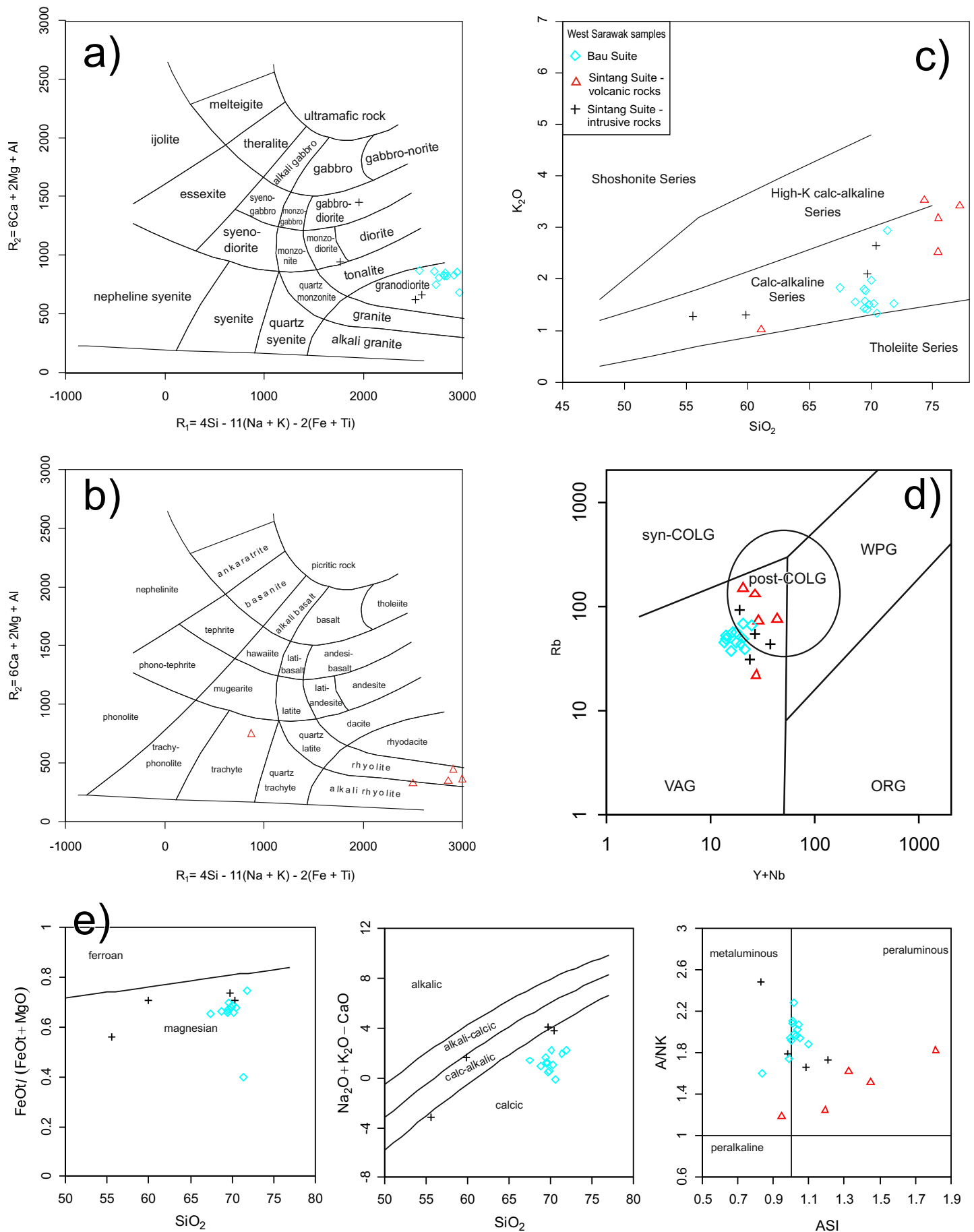


Fig. 10

| Group                          | West Sarawak Sintang Suite |                   |                   |                          |                   |                   |                         |                   |                    | Bau Suite         |                   |                    |                    |                    |                    |                    |                    |                    |                    |                    | ± 2sd              | % 2sd              |       |       |   |
|--------------------------------|----------------------------|-------------------|-------------------|--------------------------|-------------------|-------------------|-------------------------|-------------------|--------------------|-------------------|-------------------|--------------------|--------------------|--------------------|--------------------|--------------------|--------------------|--------------------|--------------------|--------------------|--------------------|--------------------|-------|-------|---|
| Sample                         | TB176b                     | TB18              | TB141             | TB209a                   | TB161             | TB58              | TB33                    | TB231             | TB23               | TB61              | TB9               | BYG1               | BYG4               | BYG5               | BYG6               | BYG8               | BYG9               | BYG10              | BYG12              | BYG13              | BYG14              | BYG15              | ± 2sd | % 2sd |   |
| Rock type                      | rhyolite                   | rhyo-<br>dacite   | rhyolite          | rhyolite                 | trachy-<br>dacite | grano-<br>diorite | micro-grano-<br>diorite | monzo-<br>diorite | gabbro-<br>diorite | grano-<br>diorite | grano-<br>diorite | grano-<br>diorite  | grano-<br>diorite  | grano-<br>diorite  | grano-<br>diorite  | grano-<br>diorite  | grano-<br>diorite  | grano-<br>diorite  | grano-<br>diorite  | grano-<br>diorite  | grano-<br>diorite  | grano-<br>diorite  |       |       | XRF<br>reproducibility<br>(estimated)** |
| Character                      | calc-<br>alkaline          | calc-<br>alkaline | calc-<br>alkaline | high-K calc-<br>alkaline | calc-<br>alkaline | calc-<br>alkaline | calc-alkaline           | calc-<br>alkaline | calc-<br>alkaline  | calc-<br>alkaline | calc-<br>alkaline | calc-<br>alkaline  | calc-<br>alkaline  | calc-<br>alkaline  | calc-<br>alkaline  | calc-<br>alkaline  | calc-<br>alkaline  | calc-<br>alkaline  | calc-<br>alkaline  | calc-<br>alkaline  | calc-<br>alkaline  | calc-<br>alkaline  |       |       |   |
| SiO <sub>2</sub>               | 77.22                      | 75.47             | 75.44             | 74.34                    | 61.09             | 70.42             | 69.72                   | 59.87             | 55.57              | 69.67             | 67.49             | 69.47              | 70.04              | 70.51              | 71.36              | 69.59              | 68.73              | 71.84              | 69.52              | 69.44              | 70.24              | 69.85              | 0.25  |       |   |
| Al <sub>2</sub> O <sub>3</sub> | 15.40                      | 14.48             | 14.97             | 15.18                    | 16.72             | 15.74             | 16.38                   | 16.57             | 17.76              | 15.78             | 16.38             | 15.68              | 14.96              | 15.81              | 14.91              | 15.70              | 15.99              | 15.24              | 15.58              | 16.00              | 15.87              | 15.69              | 0.12  |       |   |
| Fe <sub>2</sub> O <sub>3</sub> | 0.44                       | 0.26              | 1.38              | 1.01                     | 5.65              | 2.33              | 2.94                    | 7.56              | 7.28               | 2.91              | 3.19              | 3.37               | 3.08               | 2.63               | 0.83               | 2.88               | 3.30               | 2.44               | 3.18               | 3.04               | 2.74               | 3.01               | 0.05  |       |   |
| MgO                            | 0.09                       | 0.06              | 0.21              | 0.22                     | 3.90              | 0.87              | 0.95                    | 2.84              | 5.13               | 1.13              | 1.51              | 1.56               | 1.27               | 1.13               | 1.13               | 1.27               | 1.50               | 0.74               | 1.41               | 1.43               | 1.28               | 1.30               | 0.04  |       |   |
| CaO                            | 0.03                       | 0.32              | 0.35              | 1.22                     | 2.18              | 2.88              | 2.36                    | 4.44              | 7.91               | 4.58              | 4.41              | 4.09               | 3.67               | 4.83               | 4.77               | 4.28               | 4.30               | 3.24               | 4.18               | 3.95               | 4.20               | 4.49               | 0.03  |       |   |
| Na <sub>2</sub> O              | 2.90                       | 4.99              | 4.34              | 3.35                     | 7.87              | 3.99              | 4.36                    | 4.75              | 3.51               | 3.61              | 3.98              | 3.89               | 3.91               | 3.34               | 3.72               | 3.75               | 3.65               | 3.92               | 3.76               | 3.83               | 3.76               | 3.58               | 0.05  | 1.0   |   |
| K <sub>2</sub> O               | 3.42                       | 3.18              | 2.52              | 3.53                     | 1.02              | 2.65              | 2.10                    | 1.30              | 1.28               | 1.41              | 1.83              | 1.43               | 1.97               | 1.33               | 2.94               | 1.78               | 1.56               | 1.53               | 1.57               | 1.80               | 1.52               | 1.51               | 0.005 | 0.3   |   |
| TiO <sub>2</sub>               | 0.102                      | 0.081             | 0.129             | 0.091                    | 0.903             | 0.327             | 0.306                   | 1.527             | 0.844              | 0.393             | 0.520             | 0.362              | 0.434              | 0.300              | 0.382              | 0.347              | 0.419              | 0.265              | 0.369              | 0.363              | 0.323              | 0.386              | 0.004 | 0.5   |   |
| MnO                            | 0.008                      | 0.011             | 0.083             | 0.073                    | 0.119             | 0.029             | 0.098                   | 0.145             | 0.121              | 0.051             | 0.046             | 0.061              | 0.061              | 0.063              | 0.038              | 0.071              | 0.064              | 0.044              | 0.074              | 0.062              | 0.062              | 0.058              | 0.003 |       |   |
| P <sub>2</sub> O <sub>5</sub>  | 0.036                      | 0.068             | 0.131             | 0.076                    | 0.281             | 0.142             | 0.128                   | 0.326             | 0.199              | 0.105             | 0.175             | 0.121              | 0.122              | 0.105              | 0.121              | 0.125              | 0.131              | 0.102              | 0.125              | 0.137              | 0.105              | 0.149              | 0.003 |       |   |
| SO <sub>3</sub>                | 0.014                      | 0.014             | 0.010             | 0.014                    | 0.017             | 0.030             | 0.017                   | 0.034             | 0.018              | 0.014             | 0.024             |                    |                    |                    |                    |                    |                    |                    |                    |                    |                    |                    | 0.005 |       |   |
| <b>Total</b>                   | <b>99.65</b>               | <b>98.93</b>      | <b>99.57</b>      | <b>99.12</b>             | <b>99.75</b>      | <b>99.41</b>      | <b>99.36</b>            | <b>99.36</b>      | <b>99.62</b>       | <b>99.65</b>      | <b>99.55</b>      | <b>100.04</b>      | <b>99.52</b>       | <b>100.05</b>      | <b>100.20</b>      | <b>99.79</b>       | <b>99.65</b>       | <b>99.36</b>       | <b>99.77</b>       | <b>100.05</b>      | <b>100.10</b>      | <b>100.02</b>      |       |       |   |
| LOI                            | 1.91                       | 0.69              | 1.98              | 1.51                     | 1.67              | 0.78              | 1.48                    | 2.63              | 0.64               | 4.03              | 2.35              | 1.81               | 4.46               | 4.87               | 0.89               | 3.40               | 1.79               | 1.30               | 1.24               | 2.73               | 0.98               | 4.27               | 0.1   |       |   |
| Ni                             | 2.1                        | 1.6               | 1.8               | 1.6                      | 55.2              | 4.5               | 7.9                     | 22.4              | 43.1               | 8.3               | 19.9              | 26.3               | 22.5               | 17.9               | 22.50              | 14.50              | 18.9               | 24.0               | 26.5               | 17.7               | 14.7               | 14.0               | 0.5   | 2.0   |   |
| Co                             | <1                         | 7                 | 9                 | 2                        | 27                | 8                 | 7                       | 19                | 31                 | 9                 | 10                |                    |                    |                    |                    |                    |                    |                    |                    |                    |                    |                    | 1.0   | 5.0   |   |
| Cr                             | <2                         | <2                | <2                | 3                        | 90                | 6                 | 6                       | 21                | 58                 | 13                | 32                | 25                 | 21                 | 16                 | 17                 | 13                 | 11                 | 3                  | 21                 | 19                 | 15                 | 8                  | 1.0   | 2.5   |   |
| V                              | 2                          | <2                | 2                 | 3                        | 136               | 26                | 26                      | 199               | 180                | 47                | 57                | 49                 | 40                 | 39                 | 33                 | 38                 | 54                 | 22                 | 41                 | 45                 | 37                 | 42                 | 1.0   | 1.5   |   |
| Sc                             | <1.2                       | 1.3               | <1.2              | 2.2                      | 15.2              | 3.7               | 3.2                     | 21.9              | 22.4               | 7.8               | 7.4               | 8.6                | 6.4                | 6.6                | 5.8                | 6.7                | 8.4                | 3.3                | 7.9                | 7.1                | 6.8                | 6.7                | 0.5   | 4.0   |   |
| Cu                             | 2                          | 1                 | 2                 | 2                        | 24                | 37                | 4                       | 74                | 26                 | 12                | 36                | 22                 | 15                 | 9                  | 3                  | 11                 | 8                  | 7                  | 17                 | 20                 | 14                 | 15                 | 0.5   | 1.0   |   |
| Zn                             | 26                         | 7                 | 32                | 50                       | 47                | 26                | 42                      | 80                | 100                | 45                | 53                | 52                 | 47                 | 46                 | 23                 | 43                 | 47                 | 38                 | 52                 | 50                 | 44                 | 51                 | 0.7   | 1.0   |   |
| As                             | 0.3                        | 0.2               | <0.2              | 1.8                      | 1.7               | 1.6               | 0.3                     | 0.9               | 0.6                | 1.2               | 0.4               |                    |                    |                    |                    |                    |                    |                    |                    |                    |                    |                    | 0.4   |       |   |
| S                              | 38                         | 7                 | 75                | 33                       | 315               | 1314              | 35                      | 98                | 66                 | 18                | 65                |                    |                    |                    |                    |                    |                    |                    |                    |                    |                    |                    | 10.0  | 4.0   |   |
| F                              | 274                        | 335               | 327               | 129                      | 329               | 249               | 158                     | 289               | 383                | 196               | 352               |                    |                    |                    |                    |                    |                    |                    |                    |                    |                    |                    | 20.0  |       |   |
| Cl                             | 59                         | 37                | 95                | 71                       | 4798              | 511               | 93                      | 312               | 715                | 69                | 52                |                    |                    | 161                |                    |                    |                    |                    |                    |                    |                    |                    | 10.0  | 4.0   |   |
| Br                             | 0.4                        | 0.4               | 0.3               | 0.4                      | 6.2               | 0.9               | 0.4                     | 0.5               | 0.5                | 0.3               | 0.1               |                    |                    |                    |                    |                    |                    |                    |                    |                    |                    |                    | 0.2   | 5.0   |   |
| Ga                             | 16.4                       | 15.0              | 16.3              | 15.6                     | 21.2              | 14.6              | 16.7                    | 19.6              | 18.2               | 15.6              | 19.0              | 16.6               | 15.9               | 15.3               | 14.8               | 17.2               | 16.8               | 15.4               | 17.2               | 16.2               | 15.8               | 16.5               | 0.4   |       |   |
| Pb                             | 23.7                       | 11.6              | 10.9              | 30.4                     | 6.1               | 15.0              | 9.3                     | 10.8              | 6.2                | 12.1              | 10.2              | 9                  | 7.1                | 8.7                | 7.7                | 10.2               | 6.8                | 8.1                | 9.0                | 8.2                | 10.2               | 7.3                | 0.3   | 1.5   |   |
| Sr                             | 96.1                       | 190.6             | 186.4             | 213.3                    | 577.3             | 326.8             | 666.7                   | 382.8             | 680.3              | 606.3             | 587.2             | 397.6              | 222.6              | 472.8              | 372.5              | 380.4              | 237.1              | 289.2              | 320.2              | 488.7              | 546.1              | 267                | 0.2   | 0.4   |   |
| Rb                             | 130                        | 76                | 72                | 148                      | 21                | 93                | 54                      | 43                | 31                 | 48                | 49                | 38                 | 64                 | 44                 | 68                 | 55                 | 43                 | 52                 | 45                 | 56                 | 51                 | 39                 | 0.1   | 0.4   |   |
| Ba                             | 464                        | 639               | 526               | 586                      | 237               | 350               | 628                     | 359               | 340                | 452               | 307               | 404                | 265                | 369                | 457                | 402                | 300                | 388                | 361                | 317                | 414                | 436                | 2.0   | 0.8   |   |
| Zr                             | 103.5                      | 70.0              | 114.6             | 67.1                     | 149.0             | 151.0             | 173.7                   | 195.6             | 117.2              | 99.6              | 154.1             | 118.7              | 165.2              | 90.6               | 142.5              | 124.1              | 143.8              | 110.9              | 128.4              | 135.7              | 93.1               | 178.4              | 0.2   | 0.5   |   |
| Nb                             | 8.4                        | 15.0              | 11.5              | 7.8                      | 6.7               | 6.3               | 9.0                     | 6.8               | 3.9                | 4.8               | 8.9               | 6.0                | 9.3                | 4.4                | 7.5                | 6.7                | 6.6                | 5.8                | 6.8                | 6.2                | 5.3                | 8.1                | 0.1   |       |   |
| Ta                             | 2.6                        | 2.1               | 1.8               | 1.8                      | <0.7              | 1.1               | 1.1                     | <0.7              | <0.7               | <0.7              | 1.1               | 0.54 <sup>a</sup>  | 0.87 <sup>a</sup>  | 0.40 <sup>a</sup>  | 0.79 <sup>a</sup>  | 0.63 <sup>a</sup>  | 0.63 <sup>a</sup>  | 0.56 <sup>a</sup>  | 0.62 <sup>a</sup>  | 0.57 <sup>a</sup>  | 0.51 <sup>a</sup>  | 0.70 <sup>a</sup>  | 0.4   |       |   |
| Mo                             | 0.5                        | 0.8               | 1.9               | <0.2                     | 0.3               | 1.2               | 0.5                     | 0.7               | 0.9                | 0.6               | 0.9               |                    |                    |                    |                    |                    |                    |                    |                    |                    |                    |                    | 0.2   |       |   |
| Th                             | 11.4                       | 5.1               | 6.2               | 8.6                      | 5.2               | 7.7               | 10.3                    | 4.7               | 5.5                | 4.3               | 6.1               | 4.5                | 7.7                | 3.2                | 7.4                | 5.7                | 5.2                | 3.2                | 5.5                | 4.7                | 3.7                | 5.8                | 0.2   |       |   |
| U                              | 4.4                        | 2.9               | 2.0               | 3.2                      | 1.6               | 3.2               | 2.6                     | 1.0               | 0.9                | 1.2               | 1.2               | 1.17 <sup>a</sup>  | 1.84 <sup>a</sup>  | 0.90 <sup>a</sup>  | 1.50 <sup>a</sup>  | 1.31 <sup>a</sup>  | 0.77 <sup>a</sup>  | 0.94 <sup>a</sup>  | 1.21 <sup>a</sup>  | 0.80 <sup>a</sup>  | 0.89 <sup>a</sup>  | 1.56 <sup>a</sup>  | 0.5   |       |   |
| Y                              | 17.9                       | 27.8              | 16.8              | 12.4                     | 20.3              | 12.6              | 17.4                    | 30.2              | 20.0               | 8.9               | 11.0              | 9.7                | 15.1               | 9                  | 13.1               | 11                 | 12.6               | 8.3                | 10.7               | 9.7                | 8.9                | 13.3               | 0.3   |       |   |
| La                             | 21.4                       | 9.0               | 20.5              | 15.8                     | 22.2              | 15.0              | 30.2                    | 15.2              | 20.5               | 12.1              | 21.9              | 18.30 <sup>a</sup> | 20.78 <sup>a</sup> | 13.23 <sup>a</sup> | 16.74 <sup>a</sup> | 18.56 <sup>a</sup> | 18.07 <sup>a</sup> | 15.90 <sup>a</sup> | 20.28 <sup>a</sup> | 18.88 <sup>a</sup> | 12.82 <sup>a</sup> | 17.72 <sup>a</sup> | 2.0   |       |   |
| Ce                             | 46                         | 24                | 46                | 33                       | 46                | 32                | 61                      | 34                | 42                 | 25                | 44                | 30.90 <sup>a</sup> | 35.79 <sup>a</sup> | 22.51 <sup>a</sup> | 28.45 <sup>a</sup> | 32.40 <sup>a</sup> | 31.43 <sup>a</sup> | 27.56 <sup>a</sup> | 34.35 <sup>a</sup> | 33.10 <sup>a</sup> | 21.75 <sup>a</sup> | 31.11 <sup>a</sup> | 3.0   |       |   |
| Nd                             | 18.2                       | 10.1              | 18.4              | 13.9                     | 21.1              | 12.6              | 23.6                    | 19.3              | 20.9               | 11.1              | 18.1              | 12.14 <sup>a</sup> | 14.68 <sup>a</sup> | 9.48 <sup>a</sup>  | 11.67 <sup>a</sup> | 13.22 <sup>a</sup> | 13.40 <sup>a</sup> | 10.85 <sup>a</sup> | 13.30 <sup>a</sup> | 13.58 <sup>a</sup> | 9.10 <sup>a</sup>  | 13.17 <sup>a</sup> | 2.0   |       |   |
| Sm                             | 4                          | 4                 | 4                 | 3                        | 5                 | 4                 | 3                       | 4                 | 4                  | 3                 | 3                 | 2.12 <sup>a</sup>  | 2.74 <sup>a</sup>  | 1.73 <sup>a</sup>  | 2.19 <sup>a</sup>  | 2.38 <sup>a</sup>  | 2.48 <sup>a</sup>  | 1.88 <sup>a</sup>  | 2.36 <sup>a</sup>  | 2.31 <sup>a</sup>  | 1.67 <sup>a</sup>  | 2.48 <sup>a</sup>  | 2.0   |       |   |
| Yb                             | 2.0                        | 2.8               | 1.7               | 1.1                      | 2.4               | 2.1               | 2.0                     | 3.3               | 2.3                | 1.7               | 1.5               | 0.89 <sup>a</sup>  | 1.31 <sup>a</sup>  | 0.60 <sup>a</sup>  | 1.18 <sup>a</sup>  | 0.85 <sup>a</sup>  | 0.80 <sup>a</sup>  | 0.45 <sup>a</sup>  | 0.87 <sup>a</sup>  | 0.53 <sup>a</sup>  | 0.60 <sup>a</sup>  | 1.14 <sup>a</sup>  | 0.7   |       |   |
| Hf                             | 4.4                        | 3.5               | 4.6               | 3.0                      | 3.6               | 4.3               | 5.2                     | 5.2               | 2.5                | 3.3               | 4.7               | 1.75 <sup>a</sup>  | 2.93 <sup>a</sup>  | 1.43 <sup>a</sup>  | 2.14 <sup>a</sup>  | 1.44 <sup>a</sup>  | 0.93 <sup>a</sup>  | 0.39 <sup>a</sup>  | 1.92 <sup>a</sup>  | 0.87 <sup>a</sup>  | 1.31 <sup>a</sup>  | 3.12 <sup>a</sup>  | 0.5   |       |   |
| Cs                             | 6                          | <1.5              | 3                 | 10                       | <1.5              | 5                 | <1.5                    | 3                 | <1.5               | 5                 | <1.5              | 1.10 <sup>a</sup>  | 5.21 <sup>a</sup>  | 1.90 <sup>a</sup>  | 2.51 <sup>a</sup>  | 2.72 <sup>a</sup>  | 1.39 <sup>a</sup>  | 1.82 <sup>a</sup>  | 1.98 <sup>a</sup>  | 2.76 <sup>a</sup>  | 2.56 <sup>a</sup>  | 9.77 <sup>a</sup>  | 1.0   |       |   |
| Eu                             |                            |                   |                   |                          |                   |                   |                         |                   |                    |                   |                   | 0.69 <sup>a</sup>  | 0.73 <sup>a</sup>  | 0.57 <sup>a</sup>  | 0.50 <sup>a</sup>  | 0.72 <sup>a</sup>  | 0.76 <sup>a</sup>  | 0.64 <sup>a</sup>  | 0.72 <sup>a</sup>  | 0.72 <sup>a</sup>  | 0.59 <sup>a</sup>  | 0.82 <sup>a</sup>  |       |       |   |
| Gd                             |                            |                   |                   |                          |                   |                   |                         |                   |                    |                   |                   | 1.87 <sup>a</sup>  | 2.57 <sup>a</sup>  | 1.57 <sup>a</sup>  | 2.08 <sup>a</sup>  | 2.05 <sup>a</sup>  | 2.26 <sup>a</sup>  | 1.53 <sup>a</sup>  | 1.98 <sup>a</sup>  | 1.86 <sup>a</sup>  | 1.50 <sup>a</sup>  | 2.31 <sup>a</sup>  |       |       |   |

| Sample  | Longitude | Latitude | Sample type | Lithology          | Location             | Number of analysed zircons | Number of zircons ages used for mean age calculation | Weighted mean age (Ma) | Error (Ma) | MSWD |
|---|-----------|----------|-------------|--------------------|----------------------|----------------------------|--|------------------------|------------|------|
| <i>Bau Suite</i>                              |           |          |             |                    |                      |                            |  |                        |            |      |
| TB61  | 110.29019 | 1.50809  | outcrop     | granodiorite       | Bt. Stapok (quarry)  | 10                         | 3  | 12.4                   | 0.9        | 1.4  |
| TB9   | 110.37502 | 1.44329  | outcrop     | granodiorite       | Bt. Stigang (quarry) | 25                         | 16   | 14.1                   | 0.1        | 0.5  |
| <i>West Sarawak Sintang Suite - volcanic</i>  |           |          |             |                    |                      |                            |  |                        |            |      |
| TB209a  | 111.69209 | 1.05622  | float       | rhyolite           | Bt. Buwaya           | 41                         | 25   | 18.6                   | 0.2        | 2    |
| TB141   | 110.18510 | 1.64817  | outcrop     | rhyolite           | Kampung Matang       | 42                         | 15   | 19.8                   | 0.3        | 1.3  |
| <i>West Sarawak Sintang Suite - intrusive</i> |           |          |             |                    |                      |                            |  |                        |            |      |
| TB33  | 110.18631 | 1.60456  | outcrop     | micro-granodiorite | G. Bawang            | 66                         | 57   | 20.1                   | 0.2        | 2.1  |
| TB58  | 111.39105 | 1.09237  | float       | granodiorite       | Bt. Kelambi (Klambi) | 51                         | 36   | 20.3                   | 0.2        | 3    |
| TB63b   | 110.32163 | 1.72548  | outcrop     | granitic sill      | Tanjung Santubong    | 86                         | 70   | 21.1                   | 0.2        | 3.5  |



Supplementary Fig. 1: a) R1-R2 classification for plutonic rocks (De La Roche et al., 1980). b) R1-R2 classification for volcanic rocks (De La Roche et al., 1980). c) Classification of Peccerillo & Taylor (1979). d) Geotectonic classification of granitoids (Pearce et al., 1984; Pearce, 1996). e) Granite classification by Frost et al. (2001).

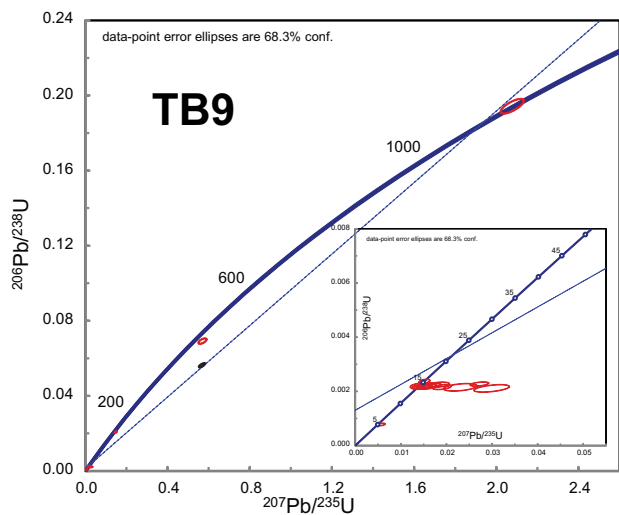
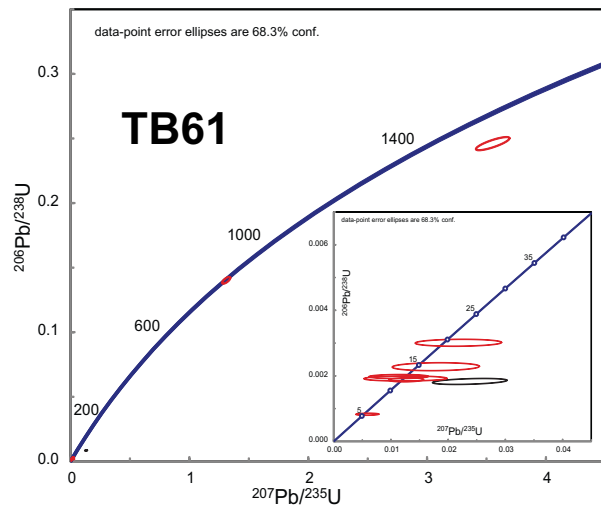
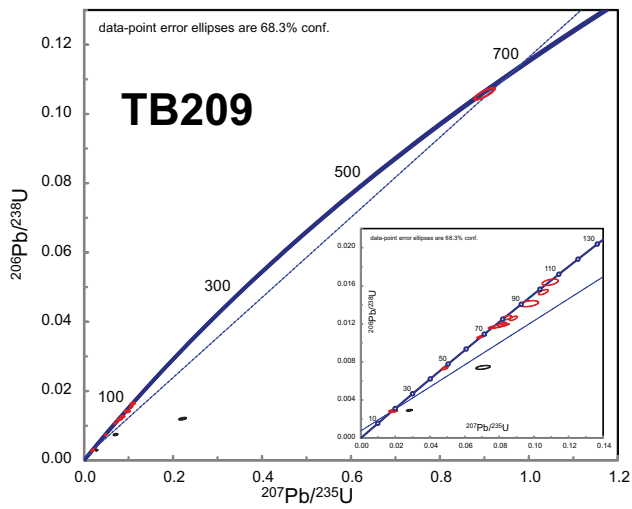
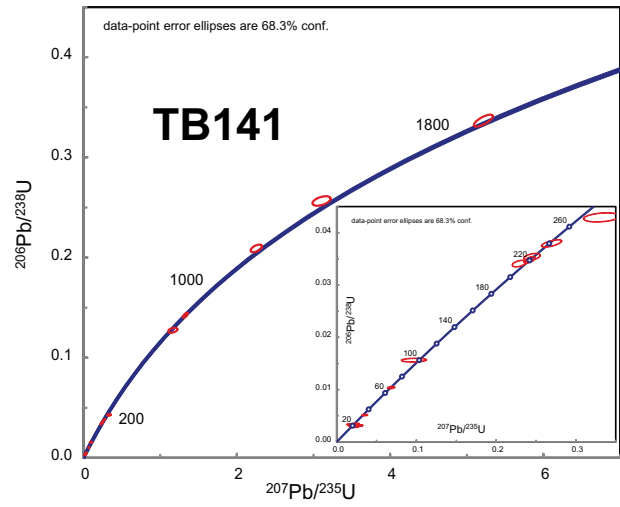
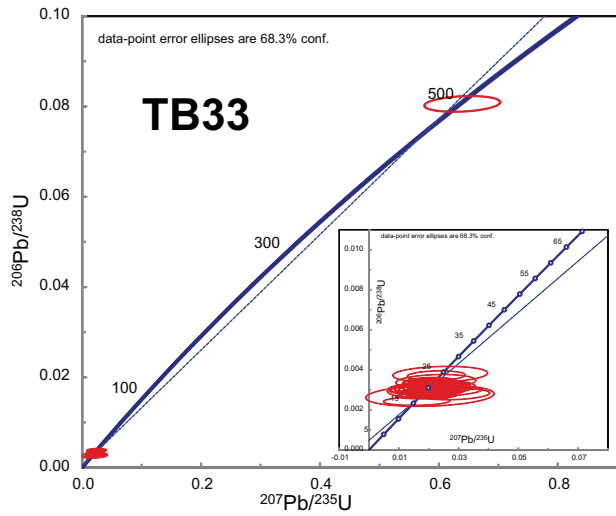
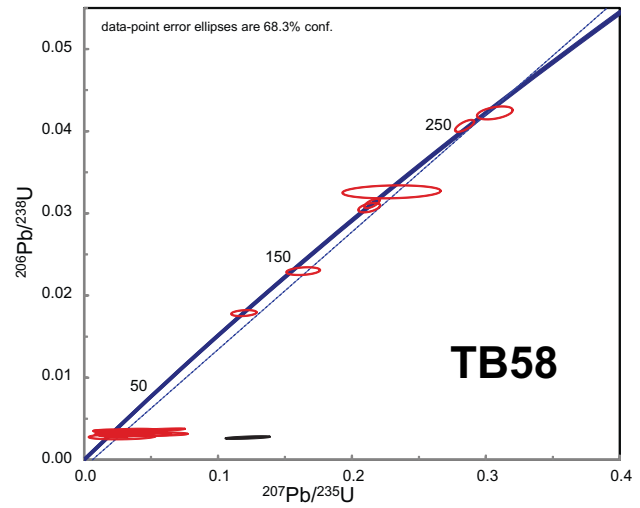
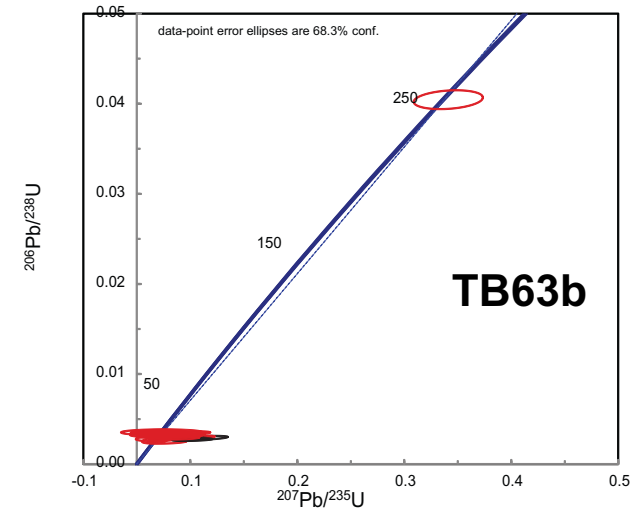
De La Roche, H., Leterrier, J., Grandclaude, P., Marchal, M., 1980. A classification of volcanic and plutonic rocks using R1-R2-diagram and major-element analyses—its relationships with current nomenclature. *Chemical Geology*, 29(1): 183-210.

Frost, B.R. et al., 2001. A Geochemical Classification for Granitic Rocks. *Journal of Petrology*, 42(11): 2033-2048.

Pearce, J., 1996. Sources and settings of granitic rocks. *Episodes*, 19: 120-125.

Pearce, J.A., Harris, N.B.W., Tindle, A.G., 1984. Trace element discrimination diagrams for the tectonic interpretation of granitic rocks. *Journal of Petrology*, 25(4): 956-983.

Peccerillo, A., Taylor, S.R., 1976. Geochemistry of Eocene calc-alkaline volcanic rocks from the Kastamonu area, northern Turkey. *Contributions to Mineralogy and Petrology*, 58(1): 63-81.



**Supplementary Fig. 2:** Concordia plots of all ages of the West Sarawak Sintang intrusive (TB63b, TB58, TB33), volcanic (TB141, TB209) and Bau Suite (TB61, TB9) rocks. Black circles are discordant results.